Journal of Medicinal Chemistry

Article

Tetra(3,4-pyrido)porphyrazines caught in the cationic cage: toward nanomolar active photosensitizers

Miloslav Machacek, Jiri Demuth, Pavel Cermak, Magda Vavreckova, Lenka Hruba, Adela Jedlickova, Pavel Kubat, Tomas Sim#nek, Veronika Novakova, and Petr Zimcik

J. Med. Chem., **Just Accepted Manuscript** • DOI: 10.1021/acs.jmedchem.6b01140 • Publication Date (Web): 28 Sep 2016

Tetra(3,4-pyrido)porphyrazines caught in the cationic cage: toward nanomolar active photosensitizers

Miloslav Machacek,† Jiri Demuth,‡ Pavel Cermak,‡ Magda Vavreckova,§ Lenka Hruba,‡ Adela Jedlickova,† Pavel Kubat,‖ Tomas Simunek,† Veronika Novakova,‡ and Petr Zimcik*,§*

†Department of Biochemical Sciences, Faculty of Pharmacy in Hradec Kralove, Charles University in Prague, Heyrovskeho 1203, Hradec Kralove, 500 05, Czech Republic

‡Department of Biophysics and Physical Chemistry, Faculty of Pharmacy in Hradec Kralove, Charles University in Prague, Heyrovskeho 1203, Hradec Kralove, 500 05, Czech Republic

§Department of Pharmaceutical Chemistry and Pharmaceutical Analysis, Faculty of Pharmacy in Hradec Kralove, Charles University in Prague, Heyrovskeho 1203, Hradec Kralove, 500 05, Czech Republic

‖J. Heyrovský Institute of Physical Chemistry, v.v.i., Academy of Sciences of the Czech Republic, Dolejškova 3, 182 23 Praha 8, Czech Republic

ABSTRACT

Investigation of a series of tetra(3,4-pyrido)porphyrazines (TPyPzs) substituted with hydrophilic substituents revealed important structure-activity relationships for their use in photodynamic therapy (PDT). Among them, a cationic TPyPz derivative with total of twelve cationic charges above, below and in the plane of the core featured a unique spatial arrangement that caught the hydrophobic core in a cage, thereby protecting it fully from aggregation in water. This derivative exhibited exceptionally effective photodynamic activity on a number of tumor cell lines (HeLa, SK-MEL-28, A549, MCF-7) with effective concentrations (EC_{50}) typically below 5 nM, at least an order of magnitude better than the EC_{50} values obtained for the clinically approved photosensitizers verteporfin, temoporfin, protoporphyrin IX and trisulfonated hydroxyaluminium phthalocyanine. Its very low dark toxicity (TC_{50} > 400 μM) and high ability to induce photodamage to endothelial cells (EA.hy926) without preincubation suggest the high potential of this cationic TPyPz derivative in vascular-targeted PDT.

INTRODUCTION

Photodynamic therapy (PDT) is a treatment modality of cancer that has been well established in clinical practice since the approval of the first drug, porfimer sodium, in 1993.[1] PDT combines three essentially non-toxic components - a photosensitizer (PS), light and oxygen. The PS absorbs the energy of the activating light and transfers it to ground-state oxygen, with subsequent formation of highly reactive singlet oxygen that destroys the target cells.[2] Even though several PSs have been clinically approved in the last twenty years, there is still room for improvement in the field of PDT to limit the toxicity and improve the efficiency of the drugs and/or increase the targeting ability of PSs to cancer cells. Several strategies have been employed to obtain more efficient and less toxic PSs. Conjugation with tumor-specific ligands (such as small molecules, peptides, proteins and antibodies) substantially increases the selectivity of the active PS toward specific cells.[3-5] The systemic toxicity may also be reduced by PSs that circulate in their inactive form in the body and are activated only by specific conditions in the tumor tissues (e.g., pH, reducing environment).[6-8] Other less traditional strategies, such as the preparation of hollow PS nanospheres[9] or dual PSs,[10] also improved the photodynamic effectiveness.

However, photodynamic treatment is already highly selective *per se* due the irradiation of target tissues only. Therefore, the improved selectivity due to the specific localization of PS appears to not be absolutely necessary unless diagnostic or theranostic effects are required.[11,12] An interesting strategy to decrease the toxicity by reducing the overall exposure to the drug appears to involve rapid elimination of the strongly hydrophilic PSs from the body at the end of the efficient treatment.[13] This approach requires highly hydrophilic PSs with rather limited protein binding as a prerequisite for rapid clearance.[14]

Phthalocyanines (Pcs) belong to a promising family of PSs with high singlet oxygen production, strong absorption over 680 nm and wide variability in substitution that may finely tune the required photophysical and physico-chemical properties.[15] For example, trisulfonated hydroxyaluminium Pc (S_3AlOHPc) has been clinically approved for PDT in Russia since 2001.[16] Additionally, the aza-analogues of Pcs, tetrapyrazinoporphyrazines[17,18] and tetra(3,4-pyrido)porphyrazines (TPyPzs)[19], are active PSs. This work focused on the synthesis and thorough *in vitro* assessment of the photodynamic properties of a group of TPyPzs substituted with hydrophilic substituents to reveal their potential in PDT in direct comparison with other clinically used PSs. The studied TPyPzs **1**-**6** (Chart 1) were functionalized with various hydrophilic moieties (anionic, cationic, or non-charged) that were attached to the core through O or S bridges with flexible (**1**-**5**) or bulky and rigid (**6**) linkers. Nitrogen as the bridging heteroatom appeared to be less suitable for PDT from a photophysical point of view.[19] In addition to the introduction of the hydrophilic moieties, the selection of the substituents allowed assessment of the effect of specific functional groups on the properties of the TPyPzs. In particular, we were interested in the inhibition of TPyPz aggregation by these substituents because this property appears to be crucial for efficient photodynamic activity of Pc-like PSs.[20]

Chart 1. Structures of the investigated TPyPzs. Only one isomer is drawn.

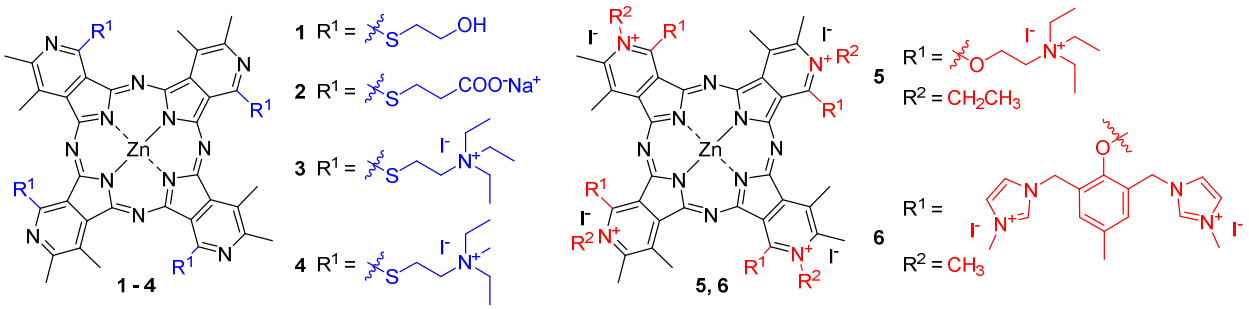

RESULTS AND DISCUSSION

Scheme 1. Synthesis of dicarbonitrile precursors and corresponding TPyPzs.[a]

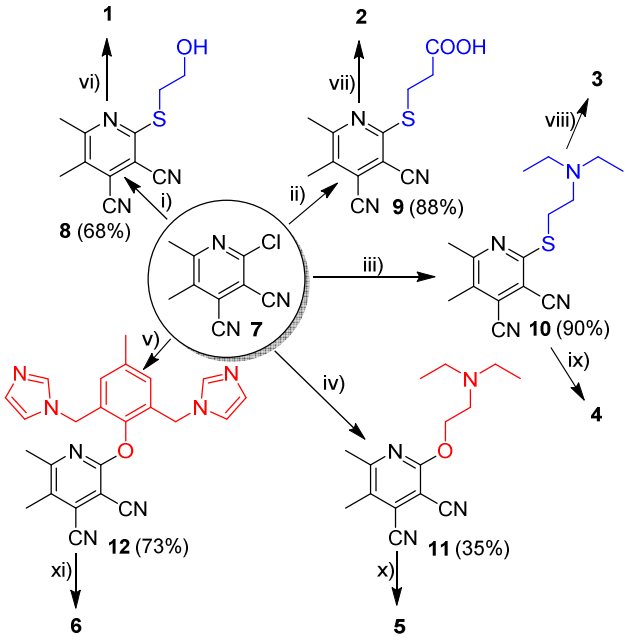

[a]Reaction conditions: i) 2-mercaptoethanol, NaOH, THF/H_2O, rt; ii) 3-mercaptopropanoic acid, K_2CO_3, DMSO, rt; iii) *N*,*N*-diethylaminoethanethiol hydrochloride, K_2CO_3, DMSO, rt; iv) *N*,*N*-diethylaminoethanol, NaH, rt, Ar; v) 2,6-bis((1*H*-imidazol-1-yl)methyl)-4-methylphenol, NaH, DMF, rt, Ar; vi) Mg, butanol, reflux, then TsOH, AcOH/H_2O, rt, then $Zn(AcO)_2$, pyridine, reflux; vii) Mg, butanol, reflux, then TsOH, THF/MeOH, rt, then $Zn(AcO)_2$, pyridine, reflux, then $NaHCO_3$; viii) Mg, butanol, reflux, then TsOH, THF/MeOH, rt, then $Zn(AcO)_2$, pyridine, reflux, then CH_3CH_2I, NMP, rt; ix) Mg, butanol, reflux, then TsOH, THF/MeOH, rt, then $Zn(AcO)_2$, pyridine, reflux, then CH_3I, NMP, rt; x) Mg, butanol, reflux, then 1% HCl, rt, then $Zn(AcO)_2$, pyridine, reflux, then CH_3CH_2I, NMP, rt; xi) Mg, butanol, reflux, then 1% HCl, rt, then $Zn(AcO)_2$, pyridine, reflux, then CH_3I, DMF, 80°C.

Synthesis. Surprisingly, since their first synthesis by Linstead in 1937,[21] the synthetic modifications of TPyPzs have been limited to the exchange of central cations and/or the quaternization of pyridine nitrogen. We only recently suggested a method for the simple functionalization of TPyPzs starting from 2-chloro-5,6-dimethylpyridine-3,4-dicarbonitrile (**7**) and thus paved the way for their rational design and fine tuning of their properties for selected applications.[19] Substituted pyridine-3,4-dicarbonitriles **8**-**12**, precursors for cyclotetramerization, were obtained from **7** by nucleophilic substitution in reasonable yields that were typically over 70% (Scheme 1). Only in the case of **11** was the yield lower, at 35%, due to the number of side products. Linstead cyclotetramerization using magnesium butoxide as the initiator was employed to obtain MgTPyPzs (mostly as a mixture of four positional isomers) because the direct template method did not produce the TPyPz ring as reported previously.[19] The metal-free ligands were released from the Mg complexes by treatment with acids and converted to Zn complexes with zinc acetate in pyridine. Compounds **3**-**6** contained quaternized peripheral moieties that originated from reaction with alkyl iodide. Significant differences in reactivity were observed during alkylation of O- and S-substituted TPyPzs. A strong electron-donating effect of alkyloxy and aryloxy substituents increased the electron density on the pyridine nitrogen of the core and consequently led to its quaternization (compounds **5** and **6**). Alkylation at both the pyridine and imidazolyl nitrogens was confirmed by signals at 54.6 ppm and 36.0 ppm, respectively, in the ^{13}C NMR of **6.** The pyridine nitrogen was not alkylated in TPyPzs bearing an S bridge (**3** and **4**).

All TPyPzs were primarily characterized by elemental analysis and MALDI-TOF spectrometry. In addition to the presence of a mixture of positional isomers, the characterization of the final TPyPzs by NMR was further complicated by their tendency to aggregate, which led

to broad and flat signals that could not be used to clearly identify **1**, **2** or **5** by NMR technique. This aggregation tendency is, however, very typical for TPyPz macrocycles, and very few papers have reported ^{1}H NMR data for this kind of compounds.[22,23] Broad but much less flat proton signals were obtained for **3** and **4**, supporting their structure. The bulkiness and rigidity of the substituted phenoxy groups resulted in sharp proton signals for both **6** and its non-alkylated macrocycle, suggesting that aggregation can be avoided in such a way. Detailed analysis of the ^{1}H NMR spectra revealed the presence of two major positional isomers C_{4h} and C_{2v} in a ratio of approximately 3:1, although a minor presence of other isomers (C_s and D_{2h}) cannot be unequivocally excluded. The prevalence of the least sterically congested isomer in the mixture is understandable considering that the extremely bulky substituted phenoxy groups cannot be easily oriented face-to-face in adjacent units. Interestingly, these isomers were not observed in the ^{13}C NMR spectrum (only one signal for each carbon was typically observed).

Absorption spectra. The absorption spectra of TPyPzs **1** and **3-6** in DMF contained the typical features of TPyPz spectra and corresponded to the prevalently monomeric form (Fig. 1). Only the absorption spectra of compound **2** indicated extensive aggregation, even in DMF. The position of the main absorption Q-band was influenced by the type of heteroatom bridge. Compounds **1-4** with sulphur as the linker typically absorbed at approximately 720 nm, whereas the O-isosteres were slightly blue-shifted by approximately 10 nm (Table 1). The shift of the Q-band agrees with the typical behavior of O- and S-substituted Pcs and their aza-analogues.[24,25] In comparison with the clinically used PSs (Table 1), TPyPzs **1-6** absorbed light of longer wavelengths, which is advantageous in PDT because of the deeper penetration of the excited light into the tissues.[2]

The planar hydrophobic core of Pcs and their analogues is typically prone to extensive self-aggregation in water.[18,26,27] Only a few rare examples of Pcs truly non-aggregating in water have been reported in the literature.[13,20,28-31] When dissolved in cell culture medium (full medium containing 10% fetal bovine serum (FBS)), TPyPzs **1-5** were characterized by a broad Q-band with a decreased extinction coefficient and the appearance of new blue-shifted bands (Fig. 1). These features indicated that the hydrophilic substituents on flexible linkers did not protect the hydrophobic cores from self-aggregation. In contrast, the rigid arrangement of quaternized imidazoles in **6**, which were forced into positions above and below the TPyPz plane, perfectly protected the macrocycle molecules from aggregating together due to electrostatic repulsive forces. Such an arrangement has been recently shown to be very efficient in hexadecacationic Pc and resulted in high photodynamic activity.[20] The advantage of TPyPz **6** lies in the additional cationic charges placed in the plane of the core on quaternized pyridines. In this way, the hydrophobic core is caught in the cage by the cationic charges and is completely protected from above, below and the side. As a consequence of this unique structural feature, no aggregation was detected in cell culture medium, even at a concentration of 500 μM (Fig. S24). The monomeric character of **6** was affected (Fig. S25) neither by changes in the ionic strength (water, buffer), by pH (from 3 to 9) nor by the presence of proteins (cell culture media).

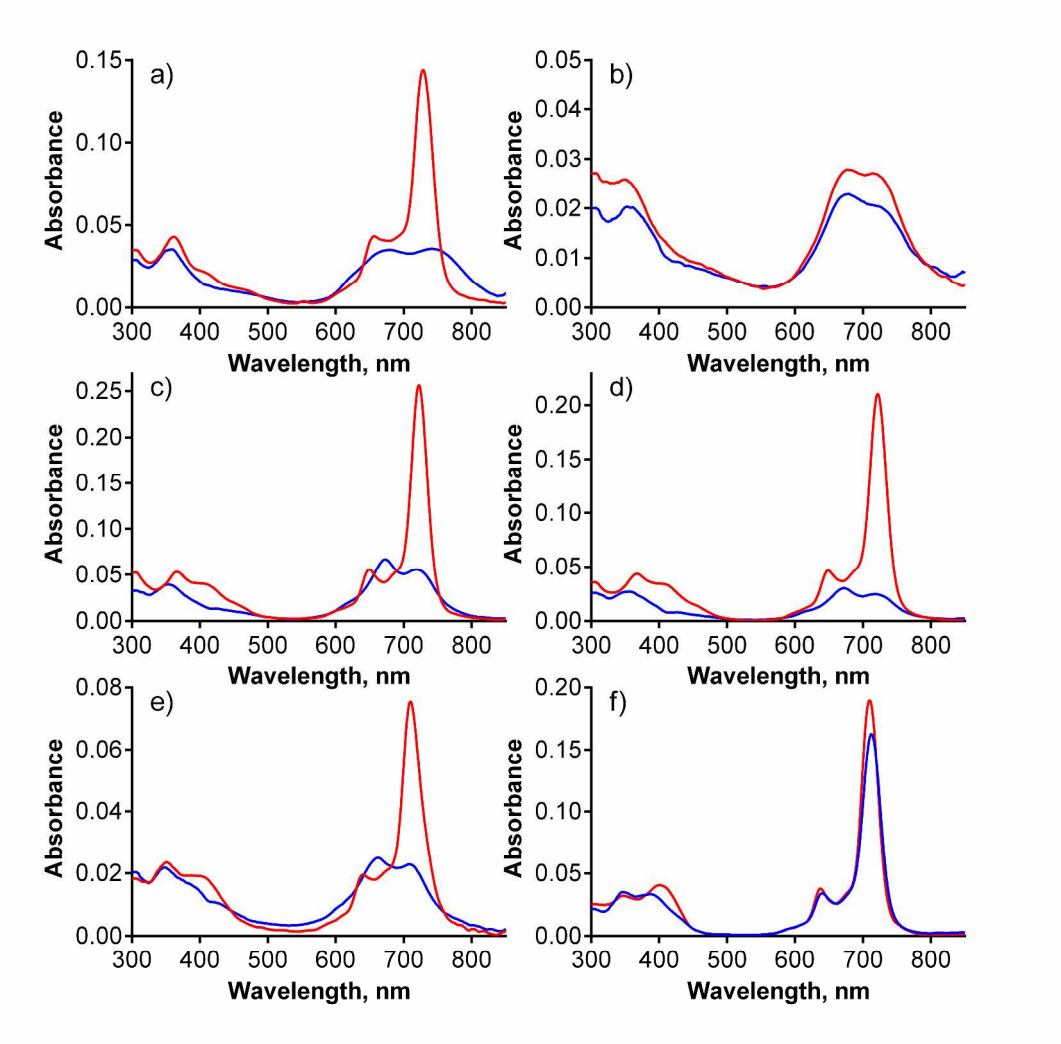

Figure 1. Absorption spectra of the studied TPyPzs **1** (a), **2** (b), **3** (c), **4** (d), **5** (e) and **6** (f) in DMF (red) and cell culture medium (blue) at a concentration of 1 μM. The samples **1**-**5** in cell culture medium were prepared from a 100 μM DMF stock solution.

Photophysical characterization. The photophysical parameters that are important for photodynamic treatment were determined primarily in DMF (Table 1). TPyPzs **1**-**6** emitted red fluorescence upon excitation, and their emission spectra were mirror images of their absorption spectra, with small Stokes shifts not exceeding 15 nm. The excitation spectra can be used for fine assessment of aggregation. They perfectly matched the absorption spectra, confirming the fully

monomeric character of **3**, **4** and **6** in DMF (Fig. S16). The slight increase in absorption at approximately 670 nm for **1** and **5** indicated a very minor contribution from aggregates that was also reflected in the lower quantum yields of these compounds (see discussion below). Compound **2** fully aggregated in DMF, as suggested above. The fluorescence quantum yields (Φ_F) were typically in the range 0.11 – 0.13 for non-aggregated **3**, **4** and **6** and were 0.09 for the slightly aggregated TPyPzs; very weak fluorescence was detected for TPyPz **2**. The fluorescence lifetimes were not greatly affected by aggregation (the signal is due only to the fluorescent species), which explains the τ_F values between 1.5 and 2 ns for all TPyPzs, including **2**.

Considering the singlet oxygen production, all TPyPzs were excellent sensitizers, with high singlet oxygen quantum yields (Φ_Δ) that reached values of approximately 0.70 for non-aggregated **3**, **4** and **6**. Similar to Φ_F, the small aggregation of **1** and **5** in DMF lowered Φ_Δ to ~ 0.42. The low Φ_Δ ~ 0.09 of **2** is due to extensive aggregation in DMF. The very small transient absorption signal of the triplet states of **2**, together with their efficient quenching by oxygen, indicated poor photogeneration of the triplet states but efficient production of singlet oxygen from these states. The lifetime of singlet oxygen (τ_Δ) in DMF varied from 9.0 to 19.3 μs, illustrating the high ability of inherent impurities to quench $O_2(^1\Delta_g)$, which is typical for DMF as the solvent.[32]

Transient absorption measurements revealed the effect of the bulky peripheral substituents in **6** that partially prevented the diffusion of oxygen to the chromophore. This effect was documented by a lower rate constant k_{O2} (Fig. S18) or a slightly lower fraction of the triplet states trapped by oxygen in **6** in an air-saturated solution (Table 1) compared to those of all other tested compounds with a relatively planar character and with no limitation of oxygen access to the core.

Although a similar effect was also observable for **6** in D_2O, it did not substantially affect the efficient production of singlet oxygen by this PS.

Water typically represents a problematic medium for various PSs due to their extensive aggregation or limited solubility (e.g., verteporfin, temoporfin and protoporphyrin IX (Pp IX) are not water soluble without a co-solvent). The Φ_F values of **6** in water were the same as in DMF, and only a slight decrease of Φ_Δ to 0.58 in D_2O was observed, suggesting that **6** retains excellent photosensitizing properties even in water.

The photophysical characterization was also performed for clinically used PSs (S_3AlOHPc, verteporfin, temoporfin, Pp IX) and methylene blue (MB) to serve as reference compounds in the following biological evaluations (Table 1).

Table 1. Absorption and photophysical data of the studied compounds.[a]

Cpd.	Solvent	λ_{max} (nm)	log ε	λ_F (nm)	τ_F (ns)	Φ_F[b]	τ_T (μs)			$10^{-9}k_{O2}$	F_T^{O2}	Φ_Δ[b]	τ_Δ (μs)
							oxygen	air	argon	($l.mol^{-1}s^{-1}$)			
1	DMF	729	5.16	744	1.75	0.09	0.096	0.45	131	3.3±0.0	0.997	0.42	15.8
2	DMF	718	4.49	736	1.89	0.01	0.081	0.42	230	4.0±0.1	0.998	~0.09	9.0
3	DMF	722	5.41	734	1.51	0.11	0.102	0.50	124	3.2±0.0	0.996	0.72	14.7
4	DMF	722	5.33	734	1.56	0.10	0.100	0.53	127	3.1±0.1	0.996	0.72	14.3
5	DMF	711	4.88	722	1.92	0.09	0.094	0.45	114	3.4±0.0	0.999	0.43	9.4
6	DMF	710	5.28	721	1.97	0.13	0.29	1.38	89	1.1±0.0	0.984	0.69	9.5
ZnPc	DMF	669[c]	-	674[c]	3.30[c]	0.28[c]	0.072	0.31	212	4.4±0.4	0.998	0.56	19.3
S_3AlOHPc	DMF	681	5.25	687	5.08	0.57	0.120	0.57	1630	2.7±0.0	1.000	0.37	19.2
verteporfin	DMF	689	4.57	694	6.12	0.14	0.061	0.29	370	3.9±0.1	0.999	0.87	18.9
Pp IX	DMF	630	3.87	633	7.61	0.04	0.081	0.42	37	3.9±0.1	0.989	0.13	19.1
temoporfin	DMF	651	4.50	655	9.29	0.20	0.083	0.42	214 (69 %) 1050 (31 %)	3.8±0.1	0.999	0.55	18.6
6	H_2O[d]	711	5.21	724	2.19	0.13	0.81	2.66	64	0.84±0.08	0.958	0.58	61.3
MB	H_2O[d]	665	4.82	685	0.40 (86%) 4.99 (14%)	0.04	0.36	1.62	113	2.0±0.1	0.986	0.52	61.1
S_3AlOHPc	H_2O[d]	679	5.17	684	5.98	0.46	0.42	1.86	833	1.7±0.1	0.999	0.37	55.3

[a]Q-band absorption maximum (λ_{max}); extinction coefficient (ε); emission maximum (λ_F); fluorescence lifetime (τ_F); fluorescence quantum yield (Φ_F); triplet state lifetime (τ_T); rate constant for quenching of triplet states by oxygen (k_{O2}); fraction of triplet states deactivated by oxygen (F_T^{O2}); singlet oxygen quantum yield (Φ_Δ); lifetime of singlet oxygen (τ_Δ). [b]The following reference compounds and values were used: MB (Φ_Δ = 0.52 in D_2O[33]), ZnPc (Φ_Δ = 0.56 in DMF[34], Φ_F = 0.32 in THF[24]). [c]Data from ref.[24]. [d]The following parameters were determined in D_2O: τ_T, k_{O2}, F_T^{O2}, Φ_Δ, τ_Δ.

***In vitro* evaluation of the dark toxicity and phototoxicity**. Comparison of the photodynamic activities of various PSs reported in the literature is typically complicated by different testing conditions, such as the irradiation (nature and energy of the light source, excitation wavelengths, bandwidth, etc.), incubation time, cell line, viability assay used, and different presentations of the results. For this reason, we evaluated a set of four clinically established PSs and MB (which is not approved but was widely studied in the past as a potential PS[35,36]) *in vitro* and directly compared their photodynamic activities under identical conditions. S_3AlOHPc is sulfonated hydroxyaluminium Pc (average degree of sulfonation, n = 3) and has been approved in Russia since 2001.[16] Temoporfin[37] and verteporfin[38] are examples of the chlorin structural family with more than fifteen years of worldwide clinical use. Pp IX, with a porphyrin macrocycle, is not used directly as a PS in PDT but represents an active form of a widely used prodrug δ-aminolevulinic acid and its esters.[39]

To demonstrate the potential of all the studied compounds in PDT, the dark toxicity (expressed as the half maximal toxic concentration, TC_{50}) and photodynamic activity (expressed as the half maximal effective concentration, EC_{50}) after irradiation ($\lambda > 570$ nm, 11.2 J/cm^2) were initially assessed on a human cervical carcinoma cell line (HeLa). Compounds **1** and **2** proved to be photodynamically ineffective under these experimental conditions due to the extensive aggregation in the cell culture medium, as stated above. Compounds **3-5** displayed high photodynamic activity (Table 2, Fig. 2a) that was comparable with several recently published Pcs and their analogues,[18] and compound **6** induced an exceptionally high photodynamic effect with $EC_{50} = 3.8 \pm 0.2$ nM. The clinically established PSs listed above proved to be significantly less effective than **6** under the same experimental conditions (Table 2, Fig. S28). Verteporfin and temoporfin were less active by an order of magnitude, whereas almost three orders of magnitude

higher EC_{50} values were determined for MB, Pp IX and $S_3AlOHPc$, making compound **6** one of the most active PS reported to date, to the best of our knowledge. For a comparison with the literature data on highly active phthalocyanine photosensitizers tested under similar conditions, see Table S1.

An effort was made to correlate the EC_{50} data of all studied compounds with their lipophilicities expressed as log *P* (Table 2). Clear increase of activity with decreased lipophilicity was observed for TPyPzs (Fig. 3a). However, this cannot be considered as the general rule for PSs since rather reverse relationship was apparent for clinically approved PSs where the most active temoporfin and verteporfin were characterized by the highest log *P* (Fig. 3a). As the singlet oxygen is supposed to be the most important cytotoxic species, the ability to produce singlet oxygen was correlated with the photodynamic activity. Expectedly, the compounds with the highest singlet oxygen production were also the most phototoxic (e.g. verteporfin, temoporfin, cpds. **3**, **4**, **6**, Fig. 3b).

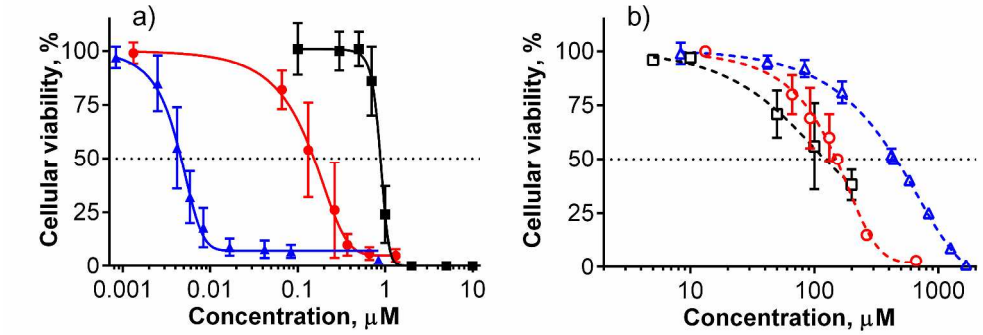

Figure 2. a) Phototoxicity (λ > 570 nm, 12.4 mW cm^{-2}, 15 min, 11.2 J cm^{-2}) and b) dark toxicity against the HeLa cells of **4** (red), **5** (black), and **6** (blue). Five independent experiments, each in quadruplicate, were typically performed.

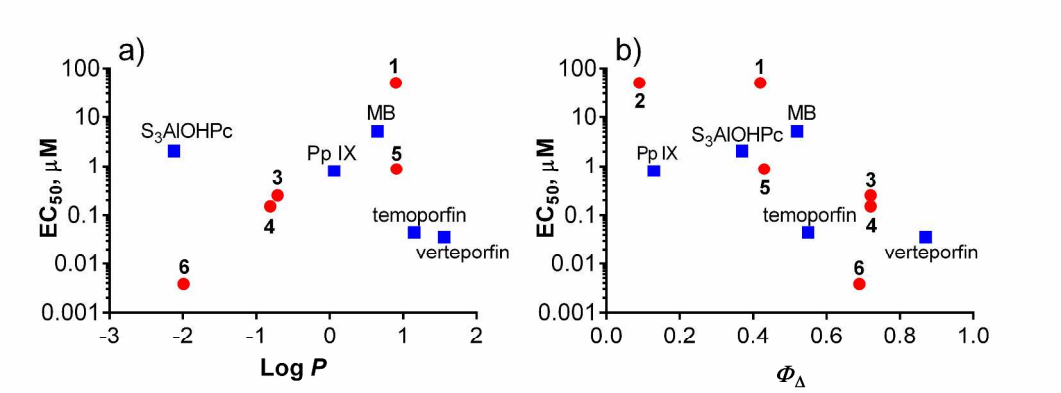

Figure 3. Dependence of photodynamic activity of studied TPyPzs (red dots) and approved PSs (blue squares) on their lipophilicity (a) or ability to produce singlet oxygen in DMF (in D_2O for MB) (b).

The dark toxicity, *i.e.,* the inherent toxicity of the compounds without irradiation, could not be determined for **1**, **2** and Pp IX due to the relatively low limit of solubility. The TC_{50} values of the other TPyPzs were over 100 μM (Fig. 2b), indicating negligible toxicity that was several times better than the toxicities of the established PSs with typical TC_{50} values of approximately 20 μM (Table 2). The latter TC_{50} values correspond well with those determined also by other groups (*e.g.* TC_{50} = 16.1 μM for temoporfin on PC-3M cells).[5] Only $S_3AlOHPc$ had TC_{50} values comparable to those of the TPyPzs. Notably, the lowest toxicity was observed for **6**, which, together with its excellent photodynamic activity, resulted in an exceptionally favourable "therapeutic ratio" TC_{50}/EC_{50} of over 110 000. This value exceeded the TC_{50}/EC_{50} of any other compound in this study by at least two orders of magnitude, making TPyPz **6** a very promising PS for the photodynamic treatment of cancerous diseases.

Table 2. Comparison of the log *P*, dark toxicity (TC_{50} values) and photodynamic activity (EC_{50} values) of the studied PSs on HeLa cells.[a]

Cpd.	log *P*	EC_{50} (μM)	TC_{50} (μM)	TC_{50}/EC_{50}
1	0.90	> 50[b]	> 50[b]	-
2	-[c]	> 50[b]	> 50[b]	-
3	-0.71	0.26 ± 0.089[d]	105 ± 9.5[d]	400
4	-0.81	0.15 ± 0.041	154 ± 4.5	1 000
5	0.91	0.87 ± 0.068	115 ± 46	130
6	-1.99	0.0038 ± 0.0002	435 ± 26	110 000
MB	0.65	5.15 ± 1.93	22.7 ± 7.9	4.4
S_3AlOHPc	-2.12	2.07 ±0.29	127 ± 7.8	60
verteporfin	1.56	0.036 ± 0.010	18.6 ± 4.2	510
Pp IX	0.06	0.80 ± 0.13	> 10[b]	> 10
temoporfin	1.15	0.045 ± 0.007	20.6 ± 2.5	460

[a]Data are presented as the TC_{50} or EC_{50} values ± standard deviations. Irradiation conditions: λ > 570 nm, 12.4 mW cm^{-2}, 15 min, 11.2 J cm^{-2}. [b]The compounds precipitated at concentrations over the listed values. [c]Could not be determined due to the precipitation. [d]Data from ref.[19]

Due to the short lifetime of singlet oxygen, the PSs only affect the biological structures in their imminent vicinity – thus, subcellular localization is crucial to understanding the processes leading to cell death upon photodynamic treatment. To evaluate the subcellular localization of **1-6**, specific fluorescent probes for mitochondria and lysosomes were employed along with the intrinsic fluorescence of the TPyPzs. All of the studied TPyPzs were located exclusively in the endo-lysosomal compartment because they were detected as punctate fluorescence co-localized with the lysosomal probe (Fig. S29). For **6**, this localization was also confirmed using live-cell laser scanning confocal microscopy (Fig. 4).

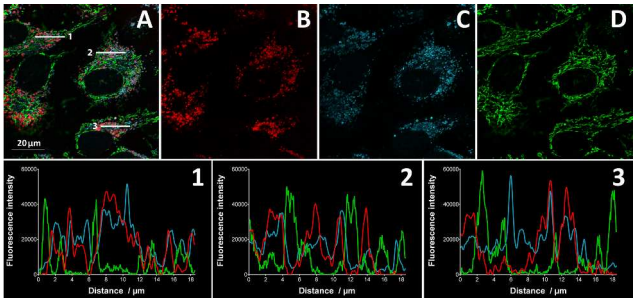

Figure 4. Subcellular localization of **6** (red, B) in HeLa cells visualized by confocal microscopy after co-incubation with the organelle-specific fluorescent probes MitoTracker (green, D) and LysoTracker (blue, C). A merged image is shown in Figure A. The lower figures show profiles of the fluorescence intensity of the corresponding parts of the confocal image in part A.

Detailed *in vitro* studies of TPyPz 6. Based on its photophysical data, low inherent toxicity and exceptional photodynamic activity, **6** was studied in more detail as the most promising candidate for PDT. Additional cytotoxicity experiments were performed on several cell lines (Fig. S28). The dark toxicity on non-malignant mouse fibroblasts (3T3) was found to be similarly very low (TC_{50} = 427 ± 54 µM). The photodynamic activity against different tumour cell lines was established using human melanoma (SK-MEL-28), human lung carcinoma (A549), human breast carcinoma (MCF-7). Here, the photodynamic effects were similar to that in HeLa cells for all malignant cell lines, reaching EC_{50} values of 3.77 ± 0.59 nM, 5.15 ± 1.57 nM and 2.83 ± 0.08 nM for SK-MEL-28, A549 and MCF-7, respectively. Much lower phototoxicity was induced on non-malignant cells, 3T3 fibroblasts and immortalised human HaCaT keratinocytes with EC_{50} = 14.9 ± 5.30 nM and 42.3 ± 6.9 nM, respectively, suggesting a certain level of selectivity for cancerous cells over healthy ones.High photodynamic effect (EC_{50} = 15.3 ± 1.8 nM, *vide infra*) was also observed against healthy permanent human umbilical vein endothelial cell line (EA.hy926) suggesting that the selectivity is not a general rule and may be important for

the selected cell lines only, *e.g.* in reducing potential skin phototoxicity due to lower effect against keratinocytes.

Interestingly, high photodynamic activity was attained by **6** at a very low intracellular concentration. The cellular uptake of **6** by HeLa cells was very rapid during the first two hours and then continued steadily for the remainder of the 12 h incubation period (Fig. 5a). The total amount of **6** after 12 h of incubation was 0.08 nmol/mg of protein in the cell lysate. When comparison was possible with other compounds studied under the same conditions, the amount of **6** was approximately seven or three times lower than the uptake of hexadecacationic Pc[20] or the hexadecaanionic aza-Pc analogue[17], respectively, that both exerted much lower photodynamic effect.

In addition to the singlet oxygen produced very efficiently even in water (Table 1), other reactive oxygen species (ROS) also contributed to the lethal effect of **6** in cells. The intracellular production of free radicals (HO•, RO•, NO_2• etc.)[40] was monitored by their quencher, chloromethyl-modified 2′,7′-dichlorodihydrofluorescein diacetate (CM-H_2DCFDA), which is reportedly insensitive to singlet oxygen.[41] As observed from Fig. 5b, the free radicals were produced only during irradiation of the cells, with negligible production of ROS before and after activation of the PS by light.

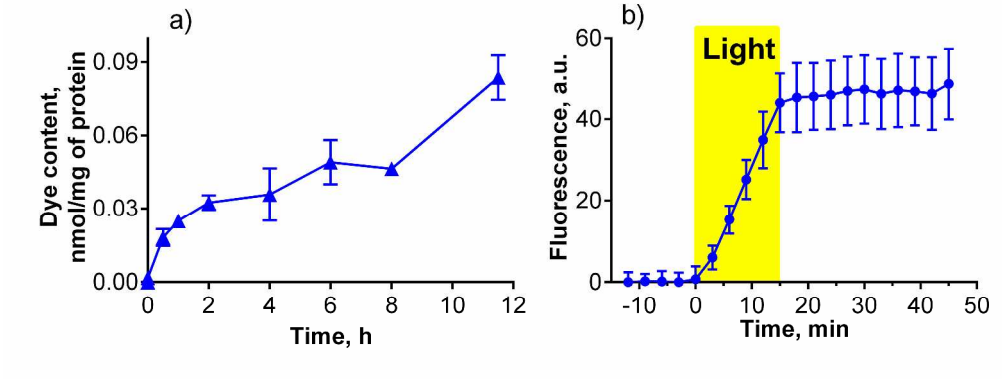

Figure 5. a) Cellular uptake of compound **6** by HeLa cells after incubation with 4 μM **6**. The experiments were performed in duplicate. b) Increase in the fluorescence of 5(6)-chloromethyl-2′,7′-dichlorofluorescein (λ_{ex} = 485 nm, λ_{em} = 525 nm) after the photodynamic treatment of HeLa cells incubated with **6**. The results were corrected for autoxidation by subtracting the light and dark controls. The experiments were performed in triplicate.

The activity of **6** could be further increased by using a longer irradiation time (Fig. 6a). Conversely, **6** was ineffective at killing cells when using a very short irradiation time (5 min) under our experimental conditions probably due to its very low concentration in the cellular compartments and the reversibility of the process at a low light dose.

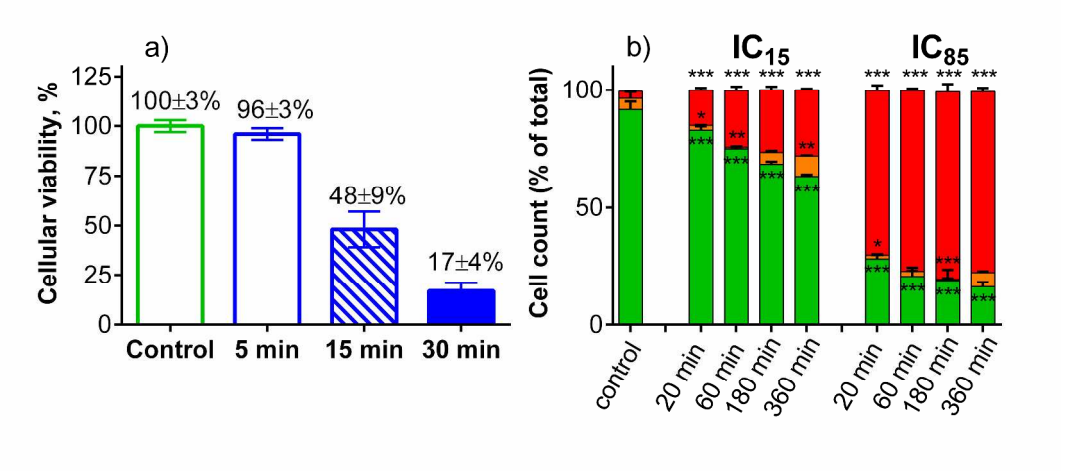

Figure 6. a) Viability of HeLa cells as a function of the light dose following photodynamic treatment with **6** (3.8 nM); green open bar, control cells (without **6** in the presence of light); blue open bar, 5 min of irradiation (total fluence 3.7 J cm^{-2}); blue dashed bar, 15 min of irradiation (11.2 J cm^{-2}); blue full bar, 30 min of irradiation (22.3 J cm^{-2}). The experiments were performed in duplicate. b) Flow cytometry assessment of the HeLa cell death mode for **6** analysed at different times after irradiation at concentrations corresponding to the EC_{15} and the EC_{85},

expressed as the cell count based on the annexin V−Alexa Fluor 488 or/and PI positivity. Non-apoptotic cells (green), apoptotic cells (orange), late apoptosis/early necrosis (red). The experiments were performed in triplicate. *, $p < 0.05$; **, $p < 0.01$; ***, $p < 0.001$.

Indeed, cells displayed a mild morphological response to oxidative insult after 5 min of irradiation. These changes were not irreversible or lethal at this length of time, and cells are probably able to recover from this damage. A longer irradiation time (over 15 min) resulted in massive cellular damage with distinct morphological features (see also Fig. 7). Cellular retraction occurred shortly after the start of irradiation (5 min) and was followed by the formation of massive membrane protrusions devoid of organelles (necrotic membrane blebs).[42] Mitochondria lost their typical filamentous structure and became spherical within 15 min of irradiation (Fig. 7). Severely damaged cell membranes became permeable to propidium iodide (PI), which passed into the cytoplasm and started to stain nuclei during the irradiation. In the post-irradiation period, nuclei shrinkage and further PI staining of chromatin were observed. We were unable to detect compound **6** by microscopic methods due to its very low intracellular concentration in this experiment until its final relocalization to the nucleus (a result of the interaction of a cationic dye with negatively charged DNA), which started 15 min after the irradiation period and ended within one hour (Fig. 7). However, considering its multicationic character and rapid damage to other organelles, we suggest that **6** was released from the lysosomes and relocalized into the other subcellular compartments within a few minutes after activation, even when it could not be easily visualized at the low concentration. All these changes observed during irradiation indicate a fast photodynamic effect of **6**. The morphological changes were corroborated by monitoring the impairment of the membranes and cytoskeleton using confocal imaging of live and fixed

specimens. The photodynamic action of **6** (at EC_{85} = 7.58 nM) resulted in complex changes – pyknosis (chromatin condensation), large membrane protrusions and reorganization of the actin and tubulin cytoskeleton (for more details see Figs. S29-S31 with corresponding discussion in the Supporting Information).

These rapid and severe morphological changes, together with the PI staining of cell nuclei that started during the irradiation period, suggest that necrosis was the main pathway of cell demise as a result of lysosomal rupture and continuous severe oxidative damage to other cellular components. Predominantly necrotic cell death has been further confirmed by flow cytometry using co-staining of the cells with PI and Annexin V-Alexa Fluor 488 – nearly no apoptotic cells were detected using both low (EC_{15}) and high (EC_{85}) doses of **6** (Fig. 6b).

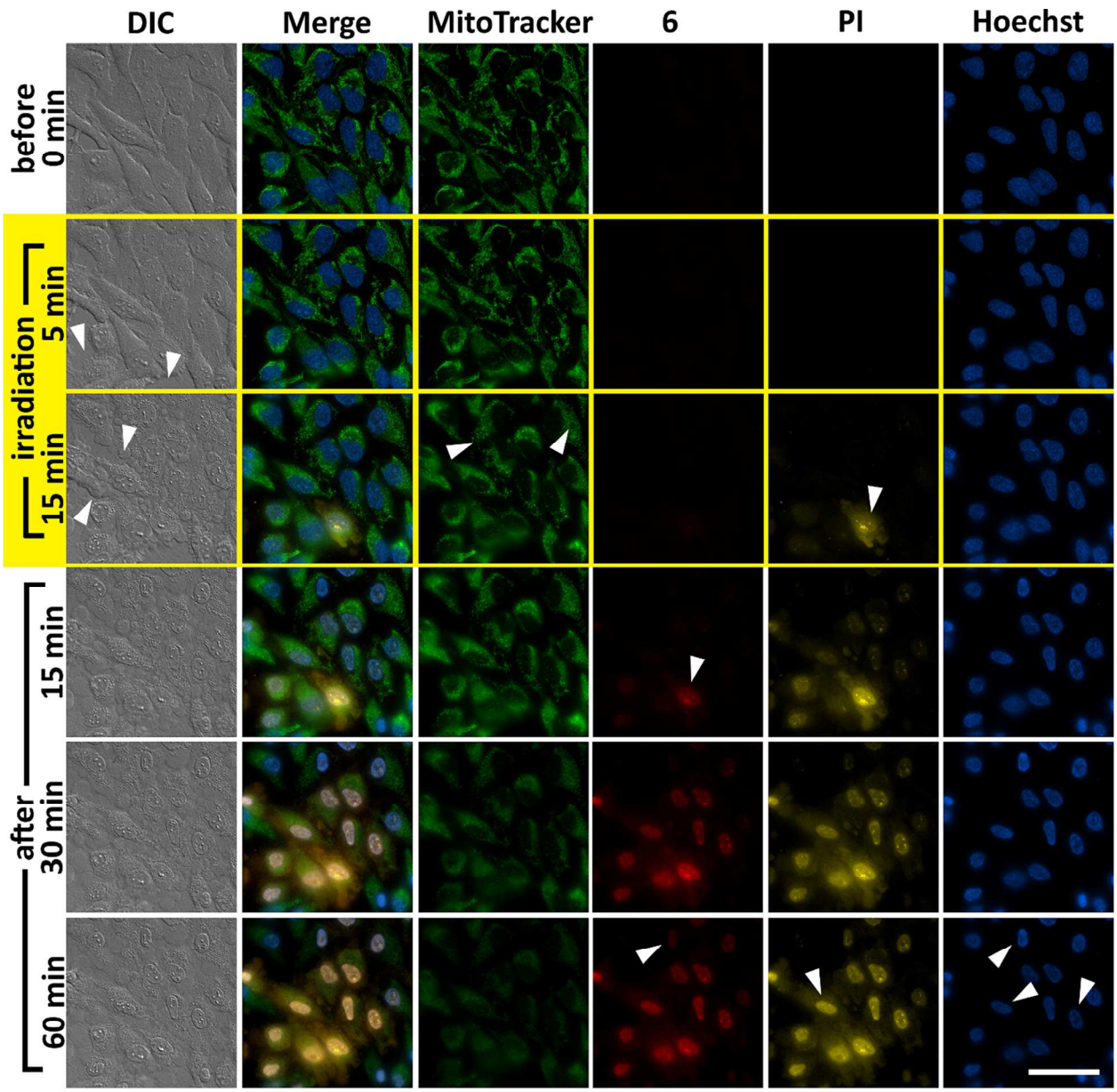

Figure 7. Changes in the morphology of HeLa cells treated with **6** during and after irradiation. The nuclei were visualized with Hoechst 33342 (Hoechst) and propidium iodide (PI); the mitochondria were visualized by MitoTracker Green. The arrows indicate important details discussed in the text. DIC = differential interference contrast. Bar represents 200 μm.

Considering that the highly hydrophilic and non-aggregating character of **6** resulted in excellent photodynamic activity at a low dose, we further assessed the potential of this compound in vascular-targeted PDT (VTP). VTP is a strategy that does not require any lag time between PS administration and irradiation and damages mainly endothelial cells, leading to tumour death primarily by vascular shutdown.[43] To evaluate whether **6** would be suitable for VTP, its phototoxicity was assessed in a permanent human umbilical vein endothelial cell line (EA.hy926) without any preincubation. In this experimental set-up, **6** still proved to be highly effective, with EC_{50} = 15.3 ± 1.8 nM. Additionally, **6** did not significantly bind to the serum proteins, as deduced from a constant fluorescence intensity and Q-band position after the addition of FBS to a solution of **6** in serum-free medium (Fig. S26). This lack of binding is a good prerequisite for rapid excretion from the body by glomerular filtration, which may limit systemic toxicity.[14]

Highly-hydrophilic compounds could be administered intravenously directly without need of any vehicle. In this case, it is crucial that drugs administered by this route do not induce any undesirable hematological effect such as drug-induced hemolysis.[44] Thus, *ex vivo* red blood cell hemolysis assay is highly recommended to determine the hemolytic potential of compounds intended for intravenous administration. Experiments with washed and diluted human erythrocytes incubated with the range of high concentration of **6** (10 – 1000 μM) were performed. No hemolysis was observed even at highest tested concentration (Fig. S27).

CONCLUSION

TPyPzs are a rather old structural group of macrocyclic dyes for which the potential in PDT has been neglected for a long time. In this study, we demonstrated that suitable structural modifications can dramatically increase the therapeutic potential of these dyes. Due to their

planar structure, TPyPzs suffer from aggregation, which is common for structurally related and more commonly studied Pcs. The aggregation of TPyPzs in water-based media cannot be easily solved using nonionic (**1**) or anionic substituents (**2**) which was also reflected in the lack of photodynamic activity. The tendency to aggregation was improved with cationic TPyPzs with flexible linkers (**3**-**5**). The EC_{50} values of these TPyPzs were only slightly higher than those of the best clinically approved PSs (verteporfin, temoporfin) and better than some of the other PSs (Pp IX, MB, S_3AlOHPc). All TPyPzs were characterized by lower inherent toxicity in the dark. Additionally, direct comparison of the photodynamic properties of the clinically approved PSs (and MB) revealed that the activity against HeLa cells under our experimental conditions decreased in the following order: verteporfin ~ temoporfin > Pp IX > S_3AlOHPc > MB.

A dramatic shift in the properties occurred when the TPyPzs were substituted non-peripherally with bulky cationic substituents, when the charges are forced above and below the macrocycle core. This arrangement is supported by additional charges in the plane of the core from the quaternized pyridine (a modification impossible for Pcs) that catch the hydrophobic TPyPz core in the cationic cage and efficiently protect the molecules by electrostatic repulsive forces from any aggregation. As a consequence, excellent photosensitizing properties of **6** were retained in water-based media without the addition of any co-solvents or surfactants and were reflected in the outstanding photodynamic activity of **6** on several different tumour cell lines with EC_{50} values typically below 5 nM. This value is an order of magnitude lower than that observed for the clinically approved PSs. Additionally, **6** was characterized by the lowest inherent toxicity (TC_{50} = 435 ± 26 μM on HeLa cells), which was at least an order of magnitude better than the toxicity of any established PS. This hydrophilic TPyPz also has potential in VTP because it efficiently destroys endothelial cells upon irradiation, even without preincubation. On the

subcellular level, this PS relocalized from lysosomes (primary target) to other organelles and eventually to the nucleus after irradiation. Impairment of the subcellular structures led to a predominantly necrosis-type cell death.

In conclusion, the versatility of the TPyPz structure enabled the development of PS **6**, which is more efficient and less toxic than any of the clinically approved PSs for PDT.

EXPERIMENTAL SECTION

General Methods. All of the organic solvents used in the synthesis were of analytical grade. Anhydrous butanol for the cyclotetramerization was freshly distilled from magnesium. Unsubstituted zinc phthalocyanine (ZnPc) was purchased from Sigma-Aldrich. All of the other chemicals for the syntheses were purchased from certified suppliers (i.e., Sigma-Aldrich, TCI Europe, Acros, and Merck) and used as received. Thin layer chromatography was performed on Merck aluminum sheets coated with silica gel 60 F254. Merck Kieselgel 60 (0.040−0.063 mm) was used for column chromatography. The melting points were measured on an Electrothermal IA9200-series digital melting-point apparatus (Electrothermal Engineering, Southend-on-Sea, Essex, Great Britain). The infrared spectra were measured on a Nicolet 6700 spectrometer in ATR mode. The ^{1}H and ^{13}C NMR spectra were recorded on a VNMR S500 NMR spectrometer. The chemical shifts are reported relative to $Si(CH_3)_4$ and were locked to the signal of the solvent. *J* values are given in Hz. The UV−Vis spectra were recorded using a Shimadzu UV-2600 spectrophotometer. Elemental analysis was carried out using a Vario Micro Cube Elemental Analyzer (Elementar Analysensysteme GmbH, Hanau, Germany). The MALDI-TOF mass spectra were recorded in positive reflectron mode on a 4800 MALDI TOF/TOF mass

spectrometer (AB Sciex, Framingham, MA, USA) in *trans*-2-[3-(4-*tert*-butylphenyl)-2-methyl-2-propenylidene]-malononitrile, which was used as a matrix. The instrument was calibrated externally with a five-point calibration using a Peptide Calibration Mix1 kit (LaserBio Laboratories, Sophia- Antipolis, France). Starting material 2-chloro-5,6-dimethylpyridine-3,4-dicarbonitrile (**7**), 2-(2-(diethylamino) ethylsulfanyl)-5,6-dimethylpyridine-3,4-dicarbonitrile (**10**), TPyPz **3** and its non-alkylated macrocyclic precursor (**3a**) were prepared according to literature.[19] All of the compounds gave satisfactory elemental analyses with a difference of ≤ 0.4% from the calculated values indicating ≥95% purity.

Preparation of 1,8,15,22-tetrakis(2-hydroxyethylsulfanyl)-3,4,10,11,17,18,24,25-octamethyltetra(3,4-pyrido)porphyrazinato zinc(II) (1). Magnesium (729 mg, 30 mmol) and a small crystal of iodine were refluxed in freshly distilled anhydrous butanol (10 mL) until all Mg was converted to magnesium butoxide (approx. 4 h). Compound **8** (989 mg, 4.2 mmol) was added, and the reflux continued for another 15 h. After cooling, the solvent was evaporated, and the product was dissolved in 50% aq. AcOH, filtered and evaporated to dryness. The dark solid was washed thoroughly with hot water, acetone and THF. Then, the product was dissolved in a small amount of pyridine and precipitated by addition of acetone. The precipitate was collected and purified on silica eluting first with MeOH to elute impurities and subsequently with pyridine:ethyl acetate 3:1 to yield 167 mg (16%) of a green solid that was characterized by MALDI-TOF (*m/z* 957.2 $[M + H]^+$; calculated for $C_{44}H_{44}MgN_{12}O_4S_4 + H^+$: 957.2). The Mg complex was directly converted to the metal-free ligand upon dissolution in 80% aq. AcOH (30 mL) with addition of *p*-toluenesulfonic acid hydrate (TsOH, 323 mg, 1.7 mmol). The mixture was stirred at rt for 4 h, the solvents were evaporated, and the dark solid was washed thoroughly with water and acetone to give a dark solid of the metal-free ligand (*m/z* 935.2 $[M + H]^+$, 917.2

[M - OH]$^+$; calculated for $C_{44}H_{46}N_{12}O_4S_4$ + H^+: 935.3). The whole product was subsequently dissolved in pyridine (10 mL) and refluxed for 4 h with zinc acetate (329 mg, 1.8 mmol). The pyridine was evaporated, and the product was washed with water and acetone. The dark solid was subsequently adsorbed onto silica, and the impurities were eluted with MeOH. The product was eluted from the silica with pyridine:ethylacetate 3:1 and evaporated to dryness to yield a dark green solid (90 mg, 9% based on **8**). Anal. Calcd. for $C_{44}H_{44}N_{12}O_4S_4Zn$ + $2H_2O$: C, 51.08; H, 4.68; N, 16.25; Found: C, 51.46; H, 4.52; N, 15.96. λ_{max} (pyridine, 1 μM)/nm 739 (ε/dm^3 mol^{-1} cm^{-1} 170 200), 663 (45 100), 365 (48 000). λ_{max} (DMF)/nm 729 (ε/dm^3 mol^{-1} cm^{-1} 144 600), 657 (43 500), 360 (43 800). IR (ATR) v = 2922 (CH), 2855 (CH), 1553, 1472, 1406, 1266, 1229, 1185, 1109, 1023 cm^{-1}. Due to aggregation, NMR spectra gave only broad and flat signals that could not be used for structure evaluation. *m/z* (MALDI TOF) 997.1 [M + H]$^+$, calculated for $C_{44}H_{44}N_{12}O_4S_4Zn$ + H^+: 997.2.

Preparation of tetrasodium salt of 1,8,15,22-tetrakis(2-carboxyethylsulfanyl)-3,4,10,11,17,18,24,25-octamethyltetra(3,4-pyrido)porphyrazinato zinc(II) (2). Magnesium (618 mg, 25 mmol) and a small crystal of iodine were refluxed in freshly distilled anhydrous butanol (30 mL) until all Mg was converted to magnesium butoxide (approx. 4 h). Compound **9** (950 mg, 3.6 mmol) was added and the reflux continued for another 4 h. After cooling, the solvent was evaporated, and 15% aq. AcOH was added (100 mL), and the mixture was stirred for 30 min at rt. The dark precipitate was collected and washed with water. The Mg complex was directly converted to metal-free ligand upon dissolution in THF:MeOH (1:1, 50 mL) with addition of TsOH (1.2 g, 6.3 mmol). The mixture was stirred at rt for 30 min, the solvents were evaporated, and the dark solid washed thoroughly with water. The whole product was subsequently dissolved in pyridine (20 mL) and refluxed for 1 h with zinc acetate (2.5 g, 13.6

mmol). The pyridine was evaporated and the product was washed with water. The solid was suspended in a small amount of THF, 10% HCl was added (100 mL) and the suspension was filtered and washed with 2% HCl and water. The product was purified by column chromatography on silica with step gradient first eluting impurities with $CHCl_3$:MeOH:AcOH 10:1:1 with subsequent elution of the product with $CHCl_3$:MeOH:AcOH 5:2:1. The product was dissolved in a mixture of 15% aq. NaOH (50 mL) and MeOH (2 mL), sonicated and filtered. The filtrate was acidified with HCl and the fine precipitate was collected and washed with water. Subsequently, the solid was dissolved in a small amount of DMF, precipitated by addition of acetone, the precipitate was collected and washed with acetone, MeOH, $CHCl_3$ and hexane to yield a dark green solid (300 mg, 46% based on **9**). The free acid was converted to its tetra sodium salt upon dissolution in 4.5 equivalents of 1 M aq. NaOH and the salt was purified by gel filtration on Sephadex G-25 eluting with water. Anal. Calcd. for $C_{48}H_{44}N_{12}O_8S_4Zn$ (free acid) + $3H_2O$: C, 49.50; H, 4.33; N, 14.43%; Found (for free acid): C, 49.83; H, 4.25; N, 14.63; No signal was detected in NMR spectra. No signal was detected in MALDI TOF MS or ESI MS in neither positive nor negative modes. λ_{max} (DMF, for tetra sodium salt **2**, 1 μM)/nm 718 (ε/dm^3 mol^{-1} cm^{-1} 30 900), 680 (28 000), 348 (26 200).

Prepration of 1,8,15,22-tetrakis(*N*,*N*,*N*-diethylmethylammonioethylsulfanyl)-3,4,10,11,17,18,24,25-octamethyltetra(3,4-pyrido)porphyrazinato zinc(II) tetraiodide (4). 1,8,15,22-tetrakis(*N*,*N*-diethylaminoethylsulfanyl)-3,4,10,11,17,18,24,25-octamethyltetra(3,4-pyrido) porphyrazinato zinc(II) (**3a**) (80 mg, 66 μmol) was dissolved in anhydrous DMF (2 mL) under argon and methyl iodide (335 mg, 2.36 mmol) was added. The mixture was heated under reflux for 24 h. The solvents were partially removed under a reduced pressure and acetone was added. Compound was subsequently several times dissolved in MeOH and precipitated by

diethylether. The green precipitate was collected and washed with diethylether, THF and acetone to yield a dark green solid (78 mg, 67%). Anal. Calcd. for $C_{64}H_{92}I_4N_{16}S_4Zn + 3H_2O$: C, 41.76; H, 5.37; N, 12.17; Found: C, 41.66; H, 5.25; N, 11.79; λ_{max} (DMF, 1 μM)/nm 722 (ε/dm^3 mol^{-1} cm^{-1} 211 400), 648 (46 900), 370 (44 500). IR (ATR) ν = 2978 (CH), 2934 (CH), 1555, 1476, 1404, 1266, 1229, 1186, 1109 cm^{-1}. ^{1}H NMR (500 MHz; CD_3SOCD_3/pyridine-D_5) δ = 4.74 – 3.69 (44 H, m, CH_2, $ArCH_3$), 3.78 – 3.56 (12 H, m, N^+CH_3), 3.20 – 2.93 (12 H, s, $ArCH_3$), 1.53 (24 H, s, CH_2CH_3). ^{1}H NMR (125 MHz; CD_3SOCD_3/pyridine-D_5) δ = 157.77, 152.30, 151.01, 148.40, 142.24, 127.00, 125.09, 59.95, 56.56, 47.54, 23.44, 21.92, 17.13, 8.45, 8.45.

Preparation of 1,8,15,22-tetrakis(*N*,*N*,*N*-triethylammonioethoxy)-2,9,16,23-tetraethyl-3,4,10,11,17,18,24,25-octamethyltetra(3,4-pyrido)porphyrazinato zinc(II) octaiodide (5). Magnesium (207 mg, 8.5 mmol) and a small crystal of iodine were refluxed in freshly distilled anhydrous butanol (10 mL) until all Mg was converted to magnesium butoxide (approx. 4 h). Compound **11** (368 mg, 1.35 mmol) was added and the reflux continued for another 15 h. After cooling, the solvent was evaporated, and the product was extracted to THF and filtered. The filtrate was concentrated to a small volume (approx. 5 mL), and precipitated by addition of acetone:hexane (1:1, 100 mL). The precipitate of the Mg complex was collected as a dark green solid, washed with acetone and characterized by MALDI-TOF MS (*m/z* 1040.6 [M – $N(C_2H_5)_2]^+$). The Mg complex was directly converted to the metal-free ligand upon dissolution in 1% HCl (50 mL). The mixture was stirred at rt for 2 h, at which time the reaction was neutralized with 10% aq. NaOH and the product precipitated. The green solid of the metal-free ligand was collected and washed with water (*m/z* 1018.5 [M – $N(C_2H_5)_2]^+$, 1091.6 [M + H]$^+$). The whole product was subsequently dissolved in pyridine (7 mL) and refluxed for 4 h with zinc acetate (110 mg, 0.6 mmol). The pyridine was evaporated, water was added with addition of

three drops of triethylamine and the precipitate was collected. The green solid was dissolved in 1% HCl, filtered and precipitated again by addition of 5% aq. $NaHCO_3$. The crude product was purified by step gradient column chromatography on neutral alumina eluting first with $CHCl_3$/THF 3:1 that eluted the impurities. The product was eluted with $CHCl_3$/MeOH 5:1. The product was obtained as a dark green viscous solid (40 mg, 11% based on **11**) (*m/z* 1053.5 $[M + H]^+$). The zinc complex was subsequently alkylated with excess of ethyl iodide (3.9 g, 25 mmol) upon dissolution in NMP (2 mL). The reaction was stirred at rt for 7 days in closed flask protected from light. Afterwards, the whole content was poured into diethylether and the precipitate was collected. The green solid was purified by repeated dissolution in MeOH, precipitation by diethylether and collection of the solid. The product was obtained as a viscous green solid (50 mg, 6% based on **11**). Anal. Calcd. for $C_{76}H_{120}I_8N_{16}O_4Zn$: C, 37.99; H, 5.03; N, 9.33; Found: C, 38.28; H, 5.05; N, 8.98; λ_{max} (DMF, 1 μM)/nm 711 (ε/dm^3 mol^{-1} cm^{-1} 76 200), 640 (19 800), 408sh, 352 (24 500). IR (ATR) ν = 2993(CH), 1590, 1448, 1275, 1200, 1131, 1098 cm^{-1}. Due to aggregation, NMR spectra gave only broad and flat signals that could not be used for structure evaluation.

Preparation of 1,8,15,22-tetrakis{2,6-bis[(3-methyl-1*H*-imidazol-3-ium-1-yl)methyl]-4-methylphenoxy}-2,3,4,9,10,11,16,17,18,23,24,25-dodecamethyltetra(3,4-pyrido)porphyrazinato zinc(II) dodecaiodide (6). Magnesium (1.0 g, 41.2 mmol) and a small crystal of iodine were refluxed in freshly distilled anhydrous butanol (85 mL) until all Mg was converted to magnesium butoxide (approx. 4 h). Compound **12** (2.5 g, 5.9 mmol) was added, and the reflux continued for another 6 h. After cooling, the solvent was evaporated, and the product was extracted with THF and $CHCl_3$, filtered and evaporated to give a dark green solid (3 g) that was characterized by MALDI-TOF MS (*m/z* 1717.6 $[M + H]^+$). The Mg complex was directly

converted to the metal-free ligand upon dissolution in 1% HCl (100 mL). The mixture was stirred at rt for 1 h, at which time the reaction was neutralized with 10% aq. NaOH and the product precipitated. The green solid of the metal-free ligand (2.4 g) was collected and washed with water (*m/z* 1695.7 $[M + H]^+$). The whole product was subsequently dissolved in pyridine (80 mL) and refluxed for 30 min with zinc acetate (1.84 g, 10 mmol). The pyridine was evaporated, and the green solid was washed with water. The dark solid was dissolved in 5% HCl and washed several times with $CHCl_3$. The water phase was collected and neutralized by addition of 10% aq. NaOH, and the green precipitate was collected and washed with water and slightly with acetone. Subsequently, the solid was dissolved in a minimal amount of $CHCl_3$ and precipitated by addition of hexane. The dark green product was collected and dried (1.5 g, 58%). Before alkylation, the product (**6a**) was characterized by MALDI-TOF MS (*m/z* 1756.5 $[M]^+$) and NMR. The ^{1}H NMR spectrum indicated the presence of the two most abundant positional isomers (C_{4h} and C_{2v}) at a ratio of approximately 3:1. Assignment of these two isomers was made on the basis of a number of signals for each proton. Only one signal is expected for C_{4h}, whereas two signals are expected for C_{2v}. Although one signal could also be expected for the D_{2h} isomer, it is very unlikely that the most congested isomer (D_{2h}) would be dominant in the mixture. Four signals typical of the C_s isomer were not observed. Data for C_{4h} isomer: ^{1}H NMR (500 MHz; $CDCl_3$/pyridine-D_5) δ = 7.46 – 7.32 (8 H, m), 7.16 (8 H, m), 7.01 – 6.94 (8 H, m), 6.76 – 6.61 (8 H, m), 5.48 – 5.29 (16 H, m, CH_2), 3.65 (12 H, s, CH_3), 2.75 – 2.63 (12 H, m, CH_3), 2.47 – 2.35 (12 H, m, CH_3). Data for C_{2v} isomer: ^{1}H NMR (500 MHz; $CDCl_3$/pyridine-D_5) δ = 7.59 – 7.55 (4 H, m), 7.55 – 7.52 (4 H, m), 7.27 – 7.24 (4 H, m), 7.23 – 7.19 (4H, m), 6.89 – 6.80 (8 H, m), 6.60 – 6.50 (8 H, m), 5.29 – 5.14 (8 H, m, CH_2),), 4.79 – 4.59 (8 H, m, CH_2), 3.84 (6 H, s, CH_3), 3.81 (6 H, s, CH_3), 2.83 (6 H, s, CH_3), 2.78 (6 H, s, CH_3), 2.34 – 2.25 (12 H, m,

CH_3). Interestingly, the methylene signal at ~ 5.2 ppm that is expected to be singlet was split due to steric congestion of the substituent and thus limited free rotation gave rise to different signals for each hydrogen. ^{13}C NMR (125 MHz; $CDCl_3$/pyridine-D_5) δ = 157.43, 155.26, 154.70, 152.36, 148.21, 146.32, 139.16, 137.23, 136.38, 133.50, 130.59, 128.45, 124.85, 119.62, 117.21, 46.55, 22.63, 21.09, 13.90. The isomers are not distinguishable in ^{13}C NMR, most of the signals of the two isomers fused together.

Compound **6a** (400 mg, 0.23 mmol) was subsequently alkylated with methyl iodide (1.16 g, 8.2 mmol) upon dissolution in anhydrous DMF (5 mL) under argon. The reaction was heated at 80°C for 24 h, the solvent was partially evaporated, and the product was precipitated by addition of acetone. The green product was collected, washed with acetone, precipitated several times by diethylether from an MeOH solution and dried (248 mg, 32%). Anal. Calcd. for $C_{108}H_{120}I_{12}N_{28}O_4Zn$: C, 37.46; H, 3.49; N, 11.33; Found: C, 37.43; H, 3.67; N, 11.64; λ_{max} (DMF, 1 μm)/nm 710 (ε/dm^3 mol^{-1} cm^{-1} 190 000), 638 (38 000), 401 (40 700). λ_{max} (H_2O)/nm 711 (ε/dm^3 mol^{-1} cm^{-1} 162 700), 640 (35 500), 384 (34 200), 346 (38 000). The ^{1}H NMR spectra indicated presence of the two most abundant positional isomers (C_{4h} and C_{2v}) at a ratio of approximately 3:1. Data for C_{4h} isomer: ^{1}H NMR (500 MHz; CD_3SOCD_3) δ = 8.96 (8 H, s), 7.74 (8 H, s), 7.44 (8 H, s), 7.42 – 7.36 (8 H, m), 5.70 – 5.61 (8 H, m, CH_2), 5.59 – 5.50 (8 H, m, CH_2), 3.53 (12 H, s, CH_3), 3.52 – 3.47 (24 H, m, imidazole NCH_3), 3.12 (12 H, s, pyridine NCH_3), 2.64 (12 H, s, CH_3), 2.60 – 2.64 (12 H, s, CH_3). Data for C_{2v} isomer: ^{1}H NMR (500 MHz; CD_3SOCD_3) δ = 8.90 – 8.83 (8 H, m), 7.81 – 7.76 (8 H, m), 7.52 – 7.47 (8 H, m), 7.32 – 7.27 (8 H, m) 6.03 – 5.91 (8 H, m, CH_2), 5.41 – 5.31 (8 H, m, CH_2), 3.83 – 3.73 (12 H, m, CH_3), 3.67 – 3.58 (24 H, m, imidazole NCH_3), some signals of C_{2v} isomer were not distinguishable as they fused with the signals of more abundant C_{4h} isomer. ^{13}C NMR (125 MHz; CD_3SOCD_3) δ =

157.17, 154.69, 154.06, 151.76, 148.75, 145.73, 136.80, 136.68, 133.20, 128.17, 124.52, 123.57, 122.52, 116.80, 54.57, 48.25, 35.99, 22.59, 20.83, 13.34. The isomers are not distinguishable in ^{13}C NMR, most of the signals of the two isomers fused together.

Preparation of 2-((2-hydroxyethylsulfanyl)-5,6-dimethylpyridine-3,4-dicarbonitrile (8). 2-Mercaptoethanol (562 mg, 0.5 mL, 7.2 mmol) was mixed with 1M aq. NaOH (7.8 mL, 7.8 mmol) and stirred at rt for 15 min. Compound **7** (1.15 g, 6 mmol) was dissolved in THF (15 mL), poured into the reaction at once and stirred at rt for 1 h. Water was added, and the product was extracted three times by ethyl acetate. The organic layer was separated, dried (Na_2SO_4), and the crude product was purified by column chromatography on silica eluting with $CHCl_3$/acetone 9:1. The purified product was crystalized from MeOH to obtain white crystals (950 mg, 68%). Mp 106.8 – 108.2 °C (from MeOH). Anal. Calcd. for $C_{11}H_{11}N_3OS$: C, 56.63; H, 4.75; N, 18.01; Found: C, 56.66; H, 4.74; N, 17.73; IR (ATR) ν = 3519 (OH), 2952 (CH), 2893 (CH), 2233 cm^{-1} (CN). ^{1}H NMR (500 MHz; $CDCl_3$) δ = 3.93 (2 H, t, J = 5.7 Hz, OCH_2), 3.48 (2 H, t, J = 5.8 Hz, SCH_2), 2.63 (3 H, s, CH_3), 2.56 (1 H, s, OH), 2.49 (3 H, s, CH_3). ^{13}C NMR (125 MHz; $CDCl_3$) δ = 162.8, 160.4, 130.3, 124.6, 113.0, 113.2, 106.1, 61.9, 33.7, 23.8, 17.0.

Preparation of 3-((3,4-dicyano-5,6-dimethylpyridin-2-yl)sulfanyl)propanoic acid (9). 3-Mercaptopropanoic acid (535 mg, 5 mmol) and K_2CO_3 (2.35 g, 17 mmol) were suspended in DMSO (10 mL) and the mixture was stirred at rt for 5 min. Solution of **7** (800 mg, 4.2 mmol) in DMSO (10 mL) was added dropwise and the mixture was stirred at rt for 1 h. Water was added (100 mL), and the mixture was made basic with few drops of NaOH solution. The water phase was washed four times with $CHCl_3$ and the organic phase was discarded. The water phase was acidified and the product was extracted three times from the water phase by ethyl acetate. The organic layer was separated, dried (Na_2SO_4), and the crude product was purified by column

chromatography on silica eluting with hexane/ethyl acetate/AcOH 10:10:1 to yield a slightly pink solid (960 mg, 88%). The product was crystallized from iPrOH. Mp 182.0 – 187.0 °C dec. (from iPrOH). Anal. Calcd. for $C_{12}H_{11}N_3O_2S$: C, 55.16; H, 4.24; N, 16.08; Found: C, 54.81; H, 4.37; N, 15.96; IR (ATR) ν = 2943 (CH), 2881 (CH), 2220 (CN), 1697 cm^{-1} (CO). ^{1}H NMR (500 MHz; CD_3COCD_3) δ = 3.55 (2 H, t, J = 6.9 Hz, SCH_2), 2.81 (2 H, t, J = 6.9 Hz, CH_2COOH), 2.70 (3 H, s, CH_3), 2.54 (3 H, s, CH_3). ^{13}C NMR (125 MHz; CD_3COCD_3) δ = 172.9, 164.4, 160.3, 131.5, 125.1, 114.4, 114.1, 106.2, 34.1, 26.2, 24.0, 17.1.

Preparation of 2-(2-(diethylamino)ethoxy)-5,6-dimethylpyridine-3,4-dicarbonitrile (11). Sodium hydride (460 mg of 60% suspension in mineral oil, 11.5 mmol) was suspended in 2-(diethylamino)ethanol (6 mL) under argon atmosphere. The mixture was stirred at rt for 15 min, at which time the compound **7** (2.0 g, 10.4 mmol) was added, and the reaction was stirred at rt for next 30 min under argon. The mixture was poured into water (100 mL), and the product was extracted three times by ethyl acetate. The organic phase was separated, acidified with HCl and the product was extracted three times by water. The organic layer was discarded, the water layer was made basic with NaOH solution and extracted three times by ethyl acetate. The organic layer was separated, dried (Na_2SO_4) and the crude product was purified by column chromatography on silica eluting with diethylether/triethylamine 30:1. The impure fractions were further purified by next column chromatography on silica with ethyl acetate/triethylamine 30:1. The product was obtained as a slightly orange solid (989 mg, 35%). Mp 60.9-62.5 °C. Anal. Calcd. for $C_{15}H_{20}N_4O$: C, 66.15; H, 7.40; N, 20.57; Found: C, 66.02; H, 7.57; N, 20.60; IR (ATR) ν = 2976 (CH), 2938 (CH), 2796 (CH), 2227 cm^{-1} (CN). ^{1}H NMR (500 MHz; $CDCl_3$) δ = 4.51 (2 H, t, J = 6.3 Hz, OCH_2), 2.87 (2 H, t, J = 6.3 Hz, NCH_2CH_2), 2.63 (4 H, q, J = 7.2 Hz, NCH_2CH_3), 2.54

(3 H, s, CH_3), 2.44 (3 H, s, CH_3), 1.06 (6 H, t, J = 7.2 Hz, CH_2CH_3). ^{13}C NMR (125 MHz; $CDCl_3$) δ = 162.4, 161.8, 126.8, 125.8, 113.5, 112.8, 95.2, 66.5, 50.9, 48.0, 23.6, 16.5, 12.0.

Preparation of 2-{2,6-bis[(1*H*-imidazol-1-yl)methyl]-4-methylphenoxy}-5,6-dimethylpyridine-3,4-dicarbonitrile (12). A flask was charged with 2,6-bis((1*H*-imidazol-1-yl)methyl)-4-methylphenol[45] (2.70 g, 10 mmol) and NaH (60% suspension in mineral oil, 400 mg, 10 mmol) and filled with argon. The mixture was dissolved in anhydrous DMF (40 mL) and stirred at rt under argon for 15 min. Compound **7** (1.60 g, 8.35 mmol) was added and the solution turned red. The mixture was stirred at rt under argon atmosphere for 18 h. Subsequently, the DMF was evaporated and the product was purified by column chromatography on silica eluting with ethyl acetate/MeOH/triethylamine 30:5:1. The product was obtained as a grey solid (2.57 g, 73%) that gave white needles after crystallization from acetone/hexane. Mp 164.4-167.8 °C (from acetone/hexane). Anal. Calcd. for $C_{24}H_{21}N_7O$: C, 68.07; H, 5.00; N, 23.15; Found: C, 67.71; H, 4.92; N, 22.75; IR (ATR) ν = 2935 (CH), 2234 cm^{-1} (CN). ^{1}H NMR (500 MHz; CD_3COCD_3) δ = 7.43 (2 H, s, imidazole CH), 7.20 (2 H, s, phenyl CH), 6.96 (2 H, s, imidazole CH), 6.76 (2 H, s, imidazole CH), 5.14 (4 H, s, CH_2), 2.46 (3 H, s, CH_3), 2.36 (3 H, s, CH_3), 2.28 (3 H, s, CH_3). ^{13}C NMR (125 MHz; CD_3COCD_3) δ = 164.7, 160.8, 146.7, 138.0, 137.9, 131.5, 131.4, 130.8, 129.5, 126.4, 120.0, 114.5, 113.5, 95.8, 46.1, 23.4, 20.9 a 16.8.

Fluorescence measurements. The steady-state and time-resolved fluorescence were measured using FS5 spectrofluorimeter (Edinburgh Instruments) equipped with TSCPC module and with extension to NIR (photomultiplier R2658P). Xe lamp was used for steady state measurements and the samples and reference compound were excited at 645 nm (**1**-**6**), 606 nm (S_3AlOHPc, MB) or at 600 nm (verteporfin, temoporfin, Pp IX). Unsubstituted zinc phthalocyanine (ZnPc) in THF was used as the reference compound for determination of fluorescence quantum yields

($\Phi_{F(ZnPc)}$ = 0.32 in THF[24]) by comparative method. The determination of Φ_F was performed in triplicate and the data represent the mean of these measurements. The estimated experimental error was 10%. Absorption of the samples at excitation wavelength was kept below 0.05 and at Q-band maximum below 0.1 to avoid inner filter effect. For time-resolved measurements, the samples were excited at 371.2 nm using EPL-375 picosecond pulsed diode laser (pulse width 68 ps).

Triplet states. Laser flash photolysis experiments were performed with a Lambda Physik FL 3002 dye laser (wavelength of 650 and 631 nm, pulse width 28 ns) pumped by COMPEX102 excimer laser. Transient absorption spectra were measured on a laser kinetic spectrometer LKS 20 (Applied Photophysics, U.K.). The kinetics of the triplet states were recorded using a 150 W Xe lamp and a R928 photomultiplier (Hamamatsu). The triplet lifetimes were measured at 500 nm for **1**-**6** and ZnPc,[46] at 420 nm for methylene blue,[47] and at 480 nm for other photosensitizers. The rate constants k_{O2} for the quenching of the triplet states by oxygen were calculated using linear Stern-Volmer equation: $1/\tau_T = 1/\tau_T^{Ar} + k_{O2}\,[O_2]$, where τ_T is lifetime of the triplet states in oxygen-, air- or argon- saturated solution. The corresponding concentrations of molecular oxygen [O_2] (3.14 mM in oxygen-saturated DMF[48] and 0.27 mM in air-saturated water[49]) were taken from the literature. Fraction of triplet states trapped by oxygen in air saturated solution was calculated as $F_T^{O2} = (\tau_T^{Ar} - \tau_T^{air})/\,\tau_T^{Ar}$.

Singlet oxygen determination. The near-infrared luminescence of singlet oxygen, $O_2(^1\Delta_g)$, at 1270 nm was monitored using a Judson Ge diode and interference filter. The samples were excited by a Lambda Physik FL3002 dye laser (λ_{exc}=650 and 631 nm). The signal from the detector was collected in a 600 MHz oscilloscope (Agilent Infiniium) and transferred to a computer for further analysis. The initial part (up to 10 μs) fails due to light scattering and strong

fluorescence, and it was not used for evaluation. The signal-to-noise ratio of the signals was improved by the averaging of 500 individual traces. The quantum yield of singlet oxygen (Φ_Δ) was estimated by the comparative method using methylene blue (MB, Φ_Δ = 0.52 in D_2O),[33] and zinc phthalocyanine (ZnPc, Φ_Δ = 0.56 in DMF[34]) as standards. Incident energy used is within the energy region, where the intensity of a luminescence signal is directly proportional to the incident energy (~150 μJ). The temporal profiles of the luminescence were fitted to a single-exponential decay function with the exclusion of the initial portion of the plot, which was affected by the formation of singlet oxygen from the triplet states of the sensitizers. This assumption is valid for lifetime of singlet oxygen $\tau_\Delta >> \tau_T$.

Determination of log*P*. Stock solutions of all PSs were prepared in DMF (in water for MB) at concentration of 100 μM. Mixture of water (400 μL) and *n*-octanol (400 μL) was prepared into plastic vial and 20 μL of the DMF stock solution of PS was added. The mixture was vortexed for 5 min at rt and then centrifuged (10 000 rpm, 10 min, rt). The octanol and water phases were separated (the middle part between the layers was discarded) and 20 μL of each layer was diluted into DMF (2 mL). Absorption spectra of these DMF solutions were measured and the log *P* was calculated: log P = log (A_{OctOH}/A_{H2O}), where A_{OctOH} and A_{H2O} are absorbances of the DMF solution at the monitoring wavelength for the *n*-octanol and water layers, respectively. The following monitoring wavelengths were used: **2** (718 nm), **3** (722 nm), **4** (722 nm), **5** (711 nm), **6** (710 nm), S_3AlOHPc (681 nm), Pp IX (409 nm), MB (663 nm), verteporfin (400 nm) and temoporfin (421 nm). Compound **1** precipitated during measurements and log *P* could not be therefore determined.

Cell cultures and samples preparation. The human cervical carcinoma (HeLa), human malignant melanoma (SK-MEL-28), human lung carcinoma (A549), human endothelial hybrid

(EA.hy926) and mouse non-malignant fibroblast (3T3) cell lines were purchased from the American Type Cell Culture Collection (ATCC; United States). The immortalised human keratinocytes (HaCaT) were obtained from Cell Lines Service (Eppelheim, Germany). The cells were cultured in Dulbecco's modified Eagle's medium (DMEM) without phenol red (Lonza, Belgium) supplemented with 10% heat-inactivated FBS (Sigma), 1% penicillin/streptomycin solution (Lonza), 10 mM HEPES buffer (Sigma, Germany), and 4 mM L-glutamine (Lonza) – further referred as cell culture or serum-containing medium (SCM). For EA.hy926, the medium was also supplemented with 2% HAT supplement (liquid mixture of 5 mM sodium hypoxanthine, 20 μM aminopterin and 0.8 mM thymidine; Gibco, Thermo Fisher Scientific, U.S.A.). The cell lines were cultured in 75 cm^2 tissue culture flasks (TPP, Switzerland) and maintained in a CO_2 incubator at 37 °C in a humidified atmosphere of 5% CO_2 and subcultured every 3−4 days. For the cytotoxicity experiments (phototoxicity and dark toxicity), the cells were seeded in 96-well plates (TPP) at a density of 7.5×10^3 (HeLa, EA.hy926) or 1.0×10^4 (SK-MEL-28, A549, 3T3, HaCaT) cells per well for 24 h.

The clinically approved photosensitizers were obtained from established suppliers: verteporfin (Sigma-Aldrich), protoporphyrin IX (Pp IX, Sigma-Aldrich), methylene blue (MB, Sigma-Aldrich), temoporfin (Cayman Chemicals). S_3AlOHPc was a kind gift from prof. Eugeny Lukyanets and was supplied as the original preparation (2 mg/mL in sterile water). For purposes of this study, the sample was lyophilized and further dissolved in cultivating medium as indicated below. According to the producer (NIOPIK, http://www.niopik.ru/products/pdt_and_fd/photosense/), S_3AlOHPc (tradename Photosens®) is sulfonated hydroxyaluminium phthalocyanine with average degree of sulfonation n = 3. The stock solutions of investigated compounds were prepared in cell culture medium at a

concentration of 1.0 mM (**6** and MB), 0.5 mM (**4**) or 2.5 mM (S_3AlOHPc, considering degree of sulfonation n = 3) or in DMSO at a concentration of 10 mM (**1**, **2**, **5**, Pp IX, verteporfin, temoporfin) and sterilized by filtration through 0.22 μm syringe filters. No change in the concentrations was detected after passage through the filter on the basis of the absorption spectra measured before and after filtration. Compound **3** has already been tested before.[19]

Cytotoxicity experiments. Dark toxicities (inherent toxicities of studied photosensitizers without a presence of any light) were assayed over a wide concentration range after 24 h incubations with HeLa cells (for **6** also with 3T3 cells). The viabilities of the cells were determined using the Neutral Red (NR) uptake assay (Sigma) based on the ability of the living cells to incorporate NR into their intact lysosomes. The soluble NR was measured as its optical density at λ = 540 nm using a Tecan Infinite 200 M plate reader (Tecan, Austria). The viability of each experimental group was expressed as the percentage of the untreated controls incubated under the same conditions (100%). After NR staining of the cells (before lysis) the cells were briefly investigated under inverted microscope to verify qualitative changes in cellular morphology and NR uptake into intact lysosomes. These observations were in accordance with subsequent quantitative measurements. False positivity in absorbance measurements using NR uptake assay method was also eliminated. After incubation with PS the cells were killed with lethal concentration of H_2O_2 (200 μM) and stained with NR uptake assay protocol used in all cellular viability experiments – no absorbance interference of any PS with NR within the whole concentration scale (PDT as well as dark toxicity experiments) was observed.

For the photodynamic treatment experiments (phototoxicity), the HeLa, SK-MEL-28, A549 or 3T3 and HaCaT cells were incubated with various concentrations of the all studied compounds for 12 h. The cells were than washed with pre-warmed serum-free medium (SFM), fresh cell

culture medium was added and the cells were irradiated for 15 min using a 450 W ozone-free Xe lamp (Newport) with intensity reduced to 400 W that was equipped with a long-pass filter (Newport OG570) and 8 cm water filter to cut-off undesirable wavelengths and heat radiation (λ > 570 nm, 12.4 mW/cm^2, 15 min, 11.2 J/cm^2). Cellular viability was measured after an additional 24 h by NR as previously described. At least five independent experiments, each in quadruplicate, were performed.

The concentrations of the tested compounds inducing a 50% viability decrease after treatment under the dark conditions (TC_{50}, the median toxic concentration) or after the photodynamic treatment (EC_{50}, the median effective concentration) were calculated using GraphPad Prism software (version 6.07; GraphPad Software, Inc., San Diego, CA) for each independent experiment. The data in Table 2 are presented as the means (± standard deviation) of these values.

In another photodynamic experiment on HeLa cells, the concentration of **6** (EC_{50} = 3.8 nM determined in the above-mentioned experiment) was fixed and the irradiation times were 5, 15 and 30 min resulting in total fluence of 3.7, 11.2 and 22.3 J/cm^2, respectively (for results see Fig 6a).

For experiment without any pre-incubation with **6** (vascular-targeted photodynamic therapy) the EA.hy926 cells were irradiated for 15 min immediately after addition of the photosensitizer. Viability was assessed after 24 h using NR.

Uptake to the cells. HeLa cells were seeded in 6 cm Petri dishes (TPP) at a density of 5.0 × 10^5 cells per dish. The cells were left to grow for 24 h, the medium was removed, and 5 mL of 4 μM **6** in cell culture medium was added. The cells were washed two times with 5 mL of pre-warmed phosphate-buffered saline (PBS; Sigma) after 0, 0.002, 0.5, 1, 2, 4, 6, 8 and 12 h. 5

mL of fresh SFM was added and cells were scraped and transferred to 15 mL centrifugation tubes (TPP) and centrifuged for 5 min at 70g. The supernatant was replaced with 2 mL of fresh SFM, and the pellet was gently resuspended and centrifuged again. This process was repeated two times. After the last centrifugation, the medium was replaced with 500 μL of MQ-water (Millipore, USA). Lysis of the cells was performed overnight at -80 °C. Samples were quickly thawed at 37°C and frozen at -80°C for additional 2 h. After quick thawing, 10 μL of 1 M hydrochloric acid was added. The fluorescence of **6** (λ_{em} = 723 nm, λ_{exc} = 342 nm) was measured using Aminco Bowman series 2 spectrofluorimeter and plotted against the incubation time. The nonspecific fluorescence was excluded by the control experiments. Calibration curve was constructed using dilution of PS stock solution in SCM with the cell lysate prepared as described above. The uptake experiments were performed in duplicate. Experiments were performed in dark the whole time.

The amount of proteins in the samples was assessed using BCA (Bicinchoninic acid) method. Calibration curve was created using bovine serum albumin (BSA) dissolved in MQ-water in the concentrations 0, 50, 100, 200, 400, 600, 800 a 1000 μg/mL. Working solution of BCA (4% $CuSO_4 \cdot 6H_2O$ mixed *ad hoc* with BSA stock solution in the 1:50 ratio) was added to 10 μl of the samples. Absorbance (562 nm) was measured after 30 min incubation at 37°C using Tecan Infinite M 200 plate reader.

Subcellular localization experiments. Approximately 7.5×10^4 HeLa cells were seeded on Petri dishes suitable for confocal microscopy (WillCo Wells, The Netherlands) in SCM and incubated for 12 h with 5 μM of **1 - 6** in an incubator (37 °C, 5% CO_2 atmosphere, constant humidity). The medium was removed, the cells were washed twice with pre-warmed PBS, and fresh medium. LysoTracker Blue DND-22 (Molecular Probes, 0.25 μM) and MitoTracker Green

FM (Molecular Probes, 0.2 μM) were added and the cells were incubated for additional 15 min. After incubation, the cells were rinsed twice with pre-warmed PBS, fresh SFM was added and the samples were immediately placed in stage top CO_2 incubator (Okolab, Italy) and examined under a Nikon Eclipse Ti-E (Nikon, Japan) fluorescence microscope equipped with an Andor Zyla cooled digital sCMOS monochromatic camera (Andor Technology, United Kingdom) and NIS Elements AR 4.20 software (Laboratory Imaging, Czech Republic). DAPI, FITC and Cy5 filter sets were used for visualization (Fig. S30). Subcellular localization of **6** was also evaluated using laser scanning confocal microscopy (LSCM). Sample was prepared the same way as described above. Nikon A1+ confocal system was employed to visualize Lysotracker Blue DND-22, MitoTracker Green FM ad **6** in live cells using 405 nm, 488 nm and 640 nm lasers respectively. One confocal plane (pinhole diameter = 26.8 μm) was taken and NIS Elements AR 4.20 software was also used to create fluorescence intensity profile.

Time-lapse DIC and fluorescence microscopy. The HeLa cells were seeded in Petri dishes suitable for confocal microscopy at the density of 7.5×10^4 cells per dish. Cells were incubated with **6** in the concentration corresponding to its EC_{85} (7.58 nM) for 12 h. Cells were co-stained for 15 min using MitoTracker Green FM (100 nM), Hoechst 33342 (4 nM) and propidium iodide (PI, 3 μM). Cells were washed two times with pre-warmed SFM and 5 mL of fresh cultivating medium containing 3 μM of PI was added. Sample was placed in stage top CO_2 incubator (humidified atmosphere of 5 % CO_2, 37°C). Irradiation was performed using the LED light source (with a Cy5 filter set) from the fluorescence microscope with power reduced to its minimum (1 %) and both ND4 and ND8 filters were used to further decrease the intensity. On the basis of the (sub)cellular morphology and the PI staining, this light source and its intensity induced the same changes as the irradiation with the Xe lamp source used in our standard

phototoxicity studies. Photomicrographs were taken using Nikon Eclipse Ti-E fluorescence microscope equipped with an Andor Zyla cooled digital sCMOS monochromatic camera and NIS Elements AR 4.20 software immediately before irradiation, at 5 and 15 min of irradiation and 15, 30 and 60 min after irradiation.

Morphology of live-cells using LSCM. For morphology changes evaluated by live-cell imaging LSCM (Fig. S30), the HeLa cells were seeded on cover glass chamber slides (Eppendorf, Germany) at the density of 2.0×10^4 cells per well and left to grow for 24 h prior to addition of **6**. Incubation with photosensitizer (at concentration of EC_{15} = 1.98 nM or EC_{85} = 7.58 nM) was performed for 12 h and irradiation was performed the same way as in phototoxicity studies. After 24 h, the cells were stained for 15 min with 0.3 μM MitoTracker Red CMXRos (Molecular Probes), 0.5× Cell Mask Green Plasma Membrane Stain (Molecular Probes) and 4 nM Hoechst 33342, washed twice with pre-warmed SFM and fresh medium was added. Sample was placed in stage top incubator and photomicrographs were taken using Nikon A1+ confocal system with 405, 488 and 561 nm lasers. DIC images were acquired using transmission detector. Five confocal focal planes were taken to cover whole volume of the cells in the field of view. Pinhole was set up at 54.9 μm and laser power was kept as low as possible to prevent undesirable photodamage.

Morphology of fixed-cells using LSCM. Seeding on cover glass chamber slides, incubation with **6** and irradiation protocol were carried out the same way as described above. Fixation of the specimens was done after 1 h (Fig. S31) and 24 h (Fig. S32) using pre-warmed 4% paraformaldehyde dissolved in SCM for 15 min at 37°C. Cells were rinsed three times for 5 min with Dulbecco's Phosphate-Buffered Saline (dPBS, pH = 7.4) and permeabilized using 0.5% Triton X-100 for 15 min at room temperature. Cells were washed three times for 5 min

with dPBS and blocked 60 min at room temperature with 3% bovine serum albumine (BSA) in dPBS. Incubation with 2.5 μg/ml α-Tubulin Antibody, Alexa Fluor® 488 conjugate (Thermo Fisher Scientific) was performed for 60 min, cells were subsequently washed three times with dPBS and 5 U/mL of Alexa Fluor® 555 phalloidin (Molecular Probes) in 3% BSA was added for additional 30 min. Specimens were rinsed and stained with 4 nM Hoechst 33342 in dPBS for 15 min and subsequently rinsed again and washed 5 min with MQ-water to remove excess salts. Mounting was performed after drying using ProLong® Gold Antifade Mountant (Molecular Probes) overnight. Photomicrographs were taken using Nikon A1 confocal system. Eight confocal planes were taken to cover whole volume of specimens using 405, 488 and 561 nm lasers. Pinhole was set up at 26.8 μm.

ROS Production Assessment. For the time profile of the ROS production of **6** at concentration corresponding to its EC_{85} value (7.58 nM), the HeLa cells were seeded in 96-well plates (TPP) at a density of 7.5×10^3 cells per well. The incubation and irradiation protocol was identical to that of the photodynamic treatment. The generation of the ROS was monitored by the intracellular conversion of the cell-permeant CM-H_2DCFDA (Molecular Probes) into a fluorescent product 5(6)-chloromethyl-2′,7′-dichlorofluorescein. The cells were incubated for 40 min in a SFM with 2.5 μM CM-H_2DCFDA. After incubation, the cells were washed two times with SFM, and fresh medium was added. The changes in the fluorescence intensity (λ_{ex} = 485 nm and λ_{em} = 525 nm) were measured using a Tecan Infinite 200 M plate reader before (12, 9, 6, 3, and 0 min), during (3, 6, 9, 12, and 15 min), and after (3−30 min in 3 min steps) irradiation under the same conditions as those in the phototoxicity experiments. Simultaneously, the experiments without an activating light (the dark control) and the experiments without the studied compounds in the presence of an activating light (the light control) were performed to

exclude the nonspecific changes in the fluorescence (primarily *via* autoxidation). The experiments were performed in triplicate.

Flow-cytometry assessment of cell-death. The HeLa cells were seeded in 60 mm Petri dishes and incubated for 12 h with **6** at concentrations corresponding to its EC_{15} (1.98 nM) and EC_{85} (7.58 nM) values. The irradiation was performed under the same conditions as those for the phototoxicity. The cells were then harvested by trypsinization followed with scraping and costained with PI (3 μM, Molecular Probes) and annexin V−Alexa Fluor 488 (1 vol %, Molecular Probes) for 15 min at room temperature. The cells that were negative or positive for red and/or green fluorescence were counted using an Accuri C6 flow cytometer (Accuri Cytometers Europe Ltd., United Kingdom) at 20, 60, 180, and 360 min after irradiation. Ten thousand events were collected per analysis. The experiment was performed in triplicate.

Preparation of erythrocytes and *ex vivo* red blood cells haemolysis assay. Whole blood (24 mL) was collected from healthy anonymous human donor directly into K_2-EDTA-coated Vacutainer tubes to prevent coagulation and processed within 1 h after collection. The whole blood was centrifuged at 750 ×g for 10 min and levels of hematocrit and plasma were marked on the tube. Plasma was aspirated gently and discarded. Hematocrit tube was filled to original level of plasma with saline, inverted a few times to gently mix and centrifuged at 750 ×g for 10 min. Washing step was repeated three times. The supernatant was aspirated and replaced with PBS at pH 7.4. Red blood cells in PBS were gently mixed by inverting the tube and diluted by PBS (dilution ratio was 1 : 2.3). 190 μL of cell culture medium (negative control), compound **6** in cell culture medium or Triton-X100 in cell culture medium (1% final concentration; positive control) was pipetted to 96-well plate with U-shaped bottom (Gama, Czech Republic). 10 μL of washed red blood cells in PBS were added and whole volume of each well was gently mixed by

pipetting. Cells were incubated at 37°C for 3 h. Whole plate was centrifuged at 750 ×g for 10 min and 50 μL of supernatant was carefully transferred to clean flat bottom 96-well plate (TPP) and 100 μL of PBS was added to each well. Absorbance was measured at 540 nm using Tecan Infinite 200 M plate reader (Tecan). Experiments without erythrocytes were also performed and their absorbance was subtracted from respective groups. Experiment was performed in triplicate.

Data analysis. The statistical analysis was performed with the GraphPad Prism statistical program (version 6.07; GraphPad Software, Inc. San Diego, CA). A one-way ANOVA test with a Bonferroni's multiple comparisons post hoc test was used. The results were compared with the control samples, and the means were considered significant if (*) $p < 0.05$, (**) $p < 0.01$, and (***) $p < 0.001$.

ASSOCIATED CONTENT

Supporting Information. NMR spectra, additional graphs and photos from photophysics and biology evaluation. This material is available free of charge via the Internet at http://pubs.acs.org.

AUTHOR INFORMATION

Corresponding Author

* petr.zimcik@faf.cuni.cz, tel. +420 495067257. * veronika.novakova@faf.cuni.cz, tel. +420 495067380.

ACKNOWLEDGMENT

This work was supported by the Czech Science Foundation (No. 13-27761S), Charles University in Prague (SVV 260 291) and the Grant Agency of Charles University (Project No. 1916214). The authors would like to thank Jiří Kuneš for the NMR measurements and Juraj Lenčo for the MALDI-TOF MS measurements. The kind donation of S_3AlOHPc from Prof. Eugeny A. Lukyanets (Russia) is gratefully acknowledged.

ABBREVIATIONS

BCA, bicinchoninic acid; CM-H_2DCFDA, chloromethyl-modified 2′,7′-dichlorodihydrofluorescein diacetate; DIC, differential interference contrast; dPBS, Dulbecco's phosphate-buffered saline; FBS, fetal bovine serum; LSCM, laser scanning confocal microscopy; MB, methylene blue; Pc, phthalocyanine; PDT, photodynamic therapy; PI, propidium iodide; PpIX, protoporphyrin IX; PS, photosensitizer; S_3AlOHPc, trisulfonated hydroxyaluminium phthalocyanine; SCM, serum-containing medium; SFM, serum-free medium; TC_{50}, half maximal toxic concentration; TPyPz, tetrapyridoporphyrazine; VTP, vascular-targeted photodynamic therapy; ZnPc, unsubstituted zinc phthalocyanine.

REFERENCES

(1) Dougherty, T. J.; Gomer, C. J.; Henderson, B. W.; Jori, G.; Kessel, D.; Korbelik, M.; Moan, J.; Peng, Q. Photodynamic therapy. *J. Natl. Cancer Inst.* **1998**, *90*, 889-905.

(2) Agostinis, P.; Berg, K.; Cengel, K. A.; Foster, T. H.; Girotti, A. W.; Gollnick, S. O.; Hahn, S. M.; Hamblin, M. R.; Juzeniene, A.; Kessel, D.; Korbelik, M.; Moan, J.; Mroz, P.; Nowis, D.; Piette, J.; Wilson, B. C.; Golab, J. Photodynamic therapy of cancer: An update. *Ca-Cancer J. Clin.* **2011**, *61*, 250-281.

(3) Luo, S. L.; Zhang, E. L.; Su, Y. P.; Cheng, T. M.; Shi, C. M. A review of NIR dyes in cancer targeting and imaging. *Biomaterials* **2011**, *32*, 7127-7138.

(4) Huang, P.; Xu, C.; Lin, J.; Wang, C.; Wang, X. S.; Zhang, C. L.; Zhou, X. J.; Guo, S. W.; Cui, D. X. Folic Acid-conjugated graphene oxide loaded with photosensitizers for targeting photodynamic therapy. *Theranostics* **2011**, *1*, 240-250.

(5) Sehgal, I.; Sibrian-Vazquez, M.; Vicente, M. G. H. Photoinduced cytotoxicity and biodistribution of prostate cancer cell-targeted porphyrins. *J. Med. Chem.* **2008**, *51*, 6014-6020.

(6) Lau, J. T. F.; Lo, P.-C.; Jiang, X.-J.; Wang, Q.; Ng, D. K. P. A dual activatable photosensitizer toward targeted photodynamic therapy. *J. Med. Chem.* **2014**, *57*, 4088-4097.

(7) Lovell, J. F.; Liu, T. W. B.; Chen, J.; Zheng, G. Activatable photosensitizers for imaging and therapy. *Chem. Rev.* **2010**, *110*, 2839-2857.

(8) He, H.; Lo, P.-C.; Ng, D. K. P. A Glutathione-activated phthalocyanine-based photosensitizer for photodynamic therapy. *Chem.–Eur. J.* **2014**, *20*, 6241-6245.

(9) Hota, R.; Baek, K.; Yun, G.; Kim, Y.; Jung, H.; Park, K. M.; Yoon, E.; Joo, T.; Kang, J.; Park, C. G.; Bae, S. M.; Ahn, W. S.; Kim, K. Self-assembled, covalently linked, hollow phthalocyanine nanospheres. *Chem. Sci.* **2013**, *4*, 339-344.

(10) Yu, Z.; Pan, W.; Li, N.; Tang, B. A nuclear targeted dual-photosensitizer for drug-resistant cancer therapy with NIR activated multiple ROS. *Chem. Sci.* **2016**, *7*, 4237-4244

(11) Lovell, J. F.; Chan, M. W.; Qi, Q.; Chen, J.; Zheng, G. Porphyrin FRET acceptors for apoptosis induction and monitoring. *J. Am. Chem. Soc.* **2011**, *133*, 18580-18582.

(12) Lobo, A. C. S.; Silva, A. D.; Tomé, V. A.; Pinto, S. M. A.; Silva, E. F. F.; Calvete, M. J. F.; Gomes, C. M. F.; Pereira, M. M.; Arnaut, L. G. Phthalocyanine labels for near-infrared fluorescence imaging of solid tumors. *J. Med. Chem.* **2016**, *59*, 4688-4696.

(13) Li, X. S.; Ke, M. R.; Zhang, M. F.; Tang, Q. Q.; Zheng, B. Y.; Huang, J. D. A non-aggregated and tumour-associated macrophage-targeted photosensitiser for photodynamic therapy: a novel zinc(II) phthalocyanine containing octa-sulphonates. *Chem. Commun.* **2015**, *51*, 4704-4707.

(14) Roberts, J. A.; Pea, F.; Lipman, J. The clinical relevance of plasma protein binding changes. *Clin. Pharmacokinet.* **2013**, *52*, 1-8.

(15) Kucinska, M.; Skupin-Mrugalska, P.; Szczolko, W.; Sobotta, L.; Sciepura, M.; Tykarska, E.; Wierzchowski, M.; Teubert, A.; Fedoruk-Wyszomirska, A.; Wyszko, E.; Gdaniec, M.; Kaczmarek, M.; Goslinski, T.; Mielcarek, J.; Murias, M. Phthalocyanine derivatives possessing 2-(morpholin-4-yl)ethoxy groups as potential agents for photodynamic therapy. *J. Med. Chem.* **2015**, *58*, 2240-2255.

(16) Lukyanets, E. A. Phthalocyanines as photosensitizers in the photodynamic therapy of cancer. *J. Porphyrins Phthalocyanines* **1999**, *3*, 424-432.

(17) Machacek, M.; Kollar, J.; Miletin, M.; Kucera, R.; Kubat, P.; Simunek, T.; Novakova, V.; Zimcik, P. Anionic hexadeca-carboxylate tetrapyrazinoporphyrazine: synthesis and in vitro photodynamic studies of a water-soluble, non-aggregating photosensitizer. *RSC Adv.* **2016**, *6*, 10064-10077.

(18) Machacek, M.; Cidlina, A.; Novakova, V.; Svec, J.; Rudolf, E.; Miletin, M.; Kučera, R.; Simunek, T.; Zimcik, P. Far-red-absorbing cationic phthalocyanine photosensitizers: synthesis and evaluation of the photodynamic anticancer activity and the mode of cell death induction. *J. Med. Chem.* **2015**, *58*, 1736-1749.

(19) Vachova, L.; Machacek, M.; Kucera, R.; Demuth, J.; Cermak, P.; Kopecky, K.; Miletin, M.; Jedlickova, A.; Simunek, T.; Novakova, V.; Zimcik, P. Heteroatom-substituted tetra(3,4-pyrido)porphyrazines: a stride toward near- infrared-absorbing macrocycles. *Org. Biomol. Chem.* **2015**, *13*, 5608-5612.

(20) Makhseed, S.; Machacek, M.; Alfadly, W.; Tuhl, A.; Vinodh, M.; Simunek, T.; Novakova, V.; Kubat, P.; Rudolf, E.; Zimcik, P. Water-soluble non-aggregating zinc phthalocyanine and in vitro studies for photodynamic therapy. *Chem. Commun.* **2013**, *49*, 11149-11151.

(21) Linstead, R. P.; Noble, E. G.; Wright, J. M. Phthalocyanines. IX. Derivatives of thiophene, thionaphthene, pyridine and pyrazine, and a note on the nomenclature *J. Chem. Soc.* **1937**, 911-921.

(22) Sakamoto, K.; Kato, T.; Cook, M. J. Position isomer separation of non-peripheral substituted zinc dibenzo-di(3,4-pyrido)porphyrazines. *J. Porphyrins Phthalocyanines* **2001**, *5*, 742-750.

(23) Ishida, Y.; Shimada, T.; Takagi, S. "Surface-fixation induced emission" of porphyrazine dye by a complexation with inorganic nanosheets. *J. Phys. Chem. C* **2014**, *118*, 20466-20471.

(24) Zimcik, P.; Novakova, V.; Kopecky, K.; Miletin, M.; Uslu Kobak, R. Z.; Svandrlikova, E.; Váchová, L.; Lang, K. Magnesium azaphthalocyanines: An emerging family of excellent red-emitting fluorophores. *Inorg. Chem.* **2012**, *51*, 4215-4223.

(25) Kobayashi, N.; Ogata, H.; Nonaka, N.; Luk'yanets, E. A. Effect of peripheral substitution on the electronic absorption and fluorescence spectra of metal-free and zinc phthalocyanines. *Chem.–Eur. J.* **2003**, *9*, 5123-5134.

(26) Nishida, M.; Horiuchi, H.; Momotake, A.; Nishimura, Y.; Hiratsuka, H.; Arai, T. Singlet molecular oxygen generation by water-soluble phthalocyanine dendrimers with different aggregation behavior. *J. Porphyrins Phthalocyanines* **2011**, *15*, 47-53.

(27) Li, X. Y.; He, X.; Ng, A. C. H.; Wu, C.; Ng, D. K. P. Influence of surfactants on the aggregation behavior of water-soluble dendritic phthalocyanines. *Macromolecules* **2000**, *33*, 2119-2123.

(28) Li, X.-S.; Guo, J.; Zhuang, J.-J.; Zheng, B.-Y.; Ke, M.-R.; Huang, J.-D. Highly positive-charged zinc(II) phthalocyanine as non-aggregated and efficient antifungal photosensitizer. *Bioorg. Med. Chem. Lett.* **2015**, *25*, 2386-2389.

(29) Liu, W.; Jensen, T. J.; Fronczek, F. R.; Hammer, R. P.; Smith, K. M.; Vicente, M. G. H. Synthesis and cellular studies of nonaggregated water-soluble phthalocyanines. *J. Med. Chem.* **2005**, *48*, 1033-1041.

(30) Lau, J. T. F.; Lo, P.-C.; Fong, W.-P.; Ng, D. K. P. Preparation and photodynamic activities of silicon(IV) phthalocyanines substituted with permethylated β-cyclodextrins. *Chem.–Eur. J.* **2011**, *17*, 7569-7577.

(31) Venkatramaiah, N.; Pereira, P. M. R.; Almeida Paz, F. A.; Ribeiro, C. A. F.; Fernandes, R.; Tome, J. P. C. Dual functionality of phosphonic-acid-appended phthalocyanines: inhibitors of urokinase plasminogen activator and anticancer photodynamic agents. *Chem. Commun.* **2015**, *51*, 15550-15553.

(32) Oelckers, S.; Hanke, T.; Röder, B. Quenching of singlet oxygen in dimethylformamide. *J. Photochem. Photobiol., A* **2000**, *132*, 29-32.

(33) Chin, K. K.; Trevithick-Sutton, C. C.; McCallum, J.; Jockusch, S.; Turro, N. J.; Scaiano, J. C.; Foote, C. S.; Garcia-Garibay, M. A. Quantitative determination of singlet oxygen generated by excited state aromatic amino acids, proteins, and immunoglobulins. *J. Am. Chem. Soc.* **2008**, *130*, 6912-6913.

(34) Michelsen, U.; Kliesch, H.; Schnurpfeil, G.; Sobbi, A. K.; Wöhrle, D. Unsymmetrically substituted benzonaphthoporphyrazines: A new class of cationic photosensitizers for the photodynamic therapy of cancer. *Photochem. Photobiol.* **1996**, *64*, 694-701.

(35) Rice, L.; Wainwright, M.; Phoenix, D. A. Phenothiazine photosensitizers. III. Activity of methylene blue derivatives against pigmented melanoma cell lines. *J. Chemother.* **2000**, *12*, 94-104.

(36) Tardivo, J. P.; Del Giglio, A.; de Oliveira, C. S.; Gabrielli, D. S.; Junqueira, H. C.; Tada, D. B.; Severino, D.; de Fátima Turchiello, R.; Baptista, M. S. Methylene blue in photodynamic therapy: From basic mechanisms to clinical applications. *Photodiagn. Photodyn. Ther.* **2005**, *2*, 175-191.

(37) Senge, M. O.; Brandt, J. C. Temoporfin (Foscan®, 5,10,15,20-tetra(*m*-hydroxyphenyl)chlorin)—A second-generation photosensitizer. *Photochem. Photobiol.* **2011**, *87*, 1240-1296.

(38) Cruess, A. F.; Zlateva, G.; Pleil, A. M.; Wirostko, B. Photodynamic therapy with verteporfin in age-related macular degeneration: a systematic review of efficacy, safety, treatment modifications and pharmacoeconomic properties. *Acta Ophthalmol.* **2009**, *87*, 118-132.

(39) Kennedy, J. C.; Pottier, R. H. Endogenous protoporphyrin IX, a clinically useful photosensitizer for photodynamic therapy. *J. Photochem. Photobiol., B* **1992**, *14*, 275-292.

(40) Halliwell, B.; Gutteridge, J. *Free Radicals in Biology and Medicine*; 4th ed.; Oxford University Press: Oxford, UK, 2007.

(41) Bilski, P.; Belanger, A. G.; Chignell, C. F. Photosensitized oxidation of 2′,7′-dichlorofluorescin: singlet oxygen does not contribute to the formation of fluorescent oxidation product 2′,7′-dichlorofluorescein, *Free Radicals Biol. Med* **2002**, *33*, 938-946.

(42) Barros, L. F.; Kanaseki, T.; Sabirov, R.; Morishima, S.; Castro, J.; Bittner, C. X.; Maeno, E.; Ando-Akatsuka, Y.; Okada, Y. Apoptotic and necrotic blebs in epithelial cells display similar neck diameters but different kinase dependency. *Cell Death Differ.* **2003**, *10*, 687-697.

(43) Azzouzi, A.-R.; Lebdai, S.; Benzaghou, F.; Stief, C. Vascular-targeted photodynamic therapy with TOOKAD® Soluble in localized prostate cancer: standardization of the procedure. *World J. Urol.* **2015**, *33*, 937-944.

(44) Dausset, J.; Contu, L. Drug-induced hemolysis *Annu. Rev. Med.* **1967**, *18*, 55-70.

(45) Yang, L.; Luo, L.; Zhang, S.; Su, X.; Lan, J.; Chen, C.-T.; You, J. Self-assembly from metal-organic vesicles to globular networks: metallogel-mediated phenylation of indole with phenyl boronic acid. *Chem. Commun.* **2010**, *46*, 3938-3940.

(46) Suchanek, J.; Lang, K.; Novakova, V.; Zimcik, P.; Zelinger, Z.; Kubat, P. Photophysical properties of CdSe quantum dot self-assemblies with zinc phthalocyanines and azaphthalocyanines. *Photochem. Photobiol. Sci.* **2013**, *12*, 743-750.

(47) Havelcova, M.; Kubat, P.; Nemcova, I. Photophysical properties of thiazine dyes in aqueous solution and in micelles. *Dyes Pigm.* **1999**, *44*, 49-54.

(48) James, H. J.; Broman, R. F. Modified winkler determination of oxygen in dimethylformamide - Oxygen solubility as a function of partial pressure. *Anal. Chim. Acta* **1969**, *48*, 411-417.

(49) Montalti, M.; Credi, A.; Prodi, L.; Gandolfi, T. M. *Handbook of Photochemistry*; 3rd ed.; CRC Press: Boca Raton, 2006.

TABLE OF CONTENTS GRAPHIC

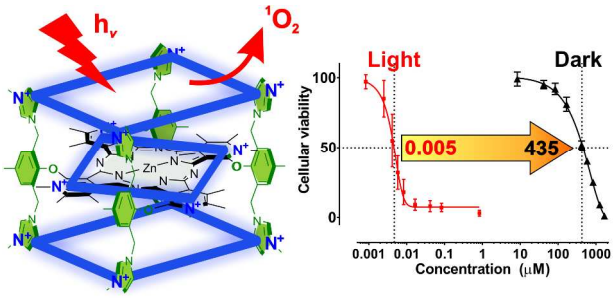

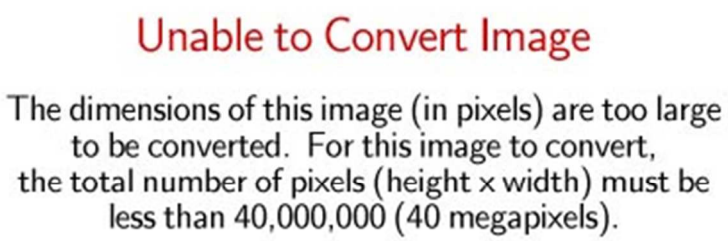

Absorption spectra of the studied TPyPzs 1 (a), 2 (b), 3 (c), 4 (d), 5 (e) and 6 (f) in DMF (red) and cell culture medium (blue) at a concentration of 1 μM. The samples 1-5 in cell culture medium were prepared from a 100 μM DMF stock solution.
Fig. 1

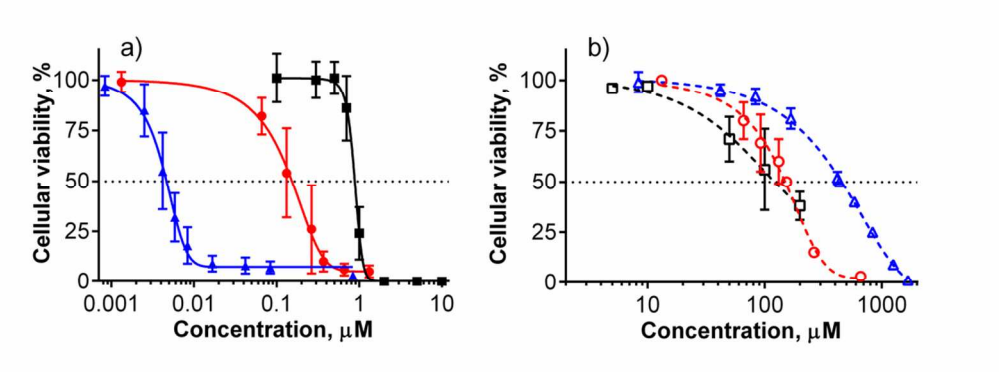

a) Phototoxicity (λ > 570 nm, 12.4 mW cm−2, 15 min, 11.2 J cm−2) and b) dark toxicity against the HeLa cells of 4 (red), 5 (black), and 6 (blue). Five independent experiments, each in quadruplicate, were typically performed.

Fig. 2

52x19mm (600 x 600 DPI)

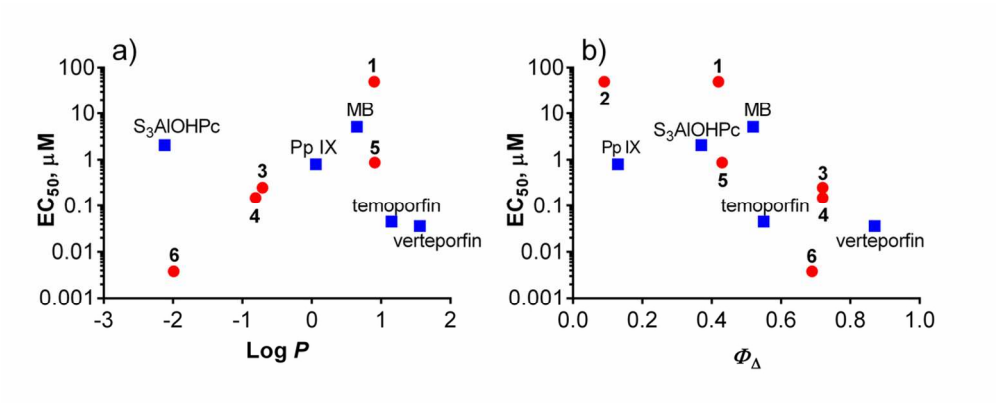

Dependence of photodynamic activity of studied TPyPzs (red dots) and approved PSs (blue squares) on their lipophilicity (a) or ability to produce singlet oxygen in DMF (in D2O for MB) (b).

Fig. 3

55x22mm (600 x 600 DPI)

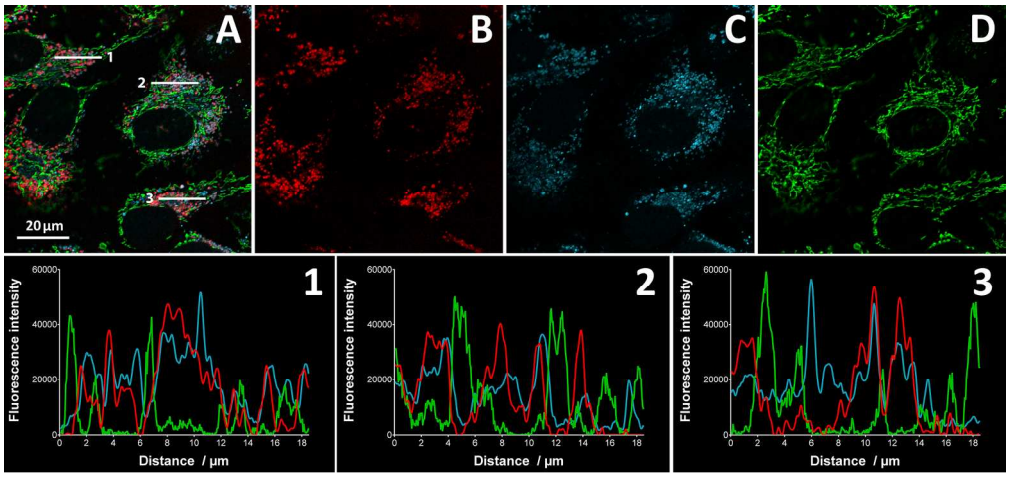

Subcellular localization of 6 (red, B) in HeLa cells visualized by confocal microscopy after co-incubation with the organelle-specific fluorescent probes MitoTracker (green, D) and LysoTracker (blue, C). A merged image is shown in Figure A. The lower figures show profiles of the fluorescence intensity of the corresponding parts of the confocal image in part A.

Fig. 4

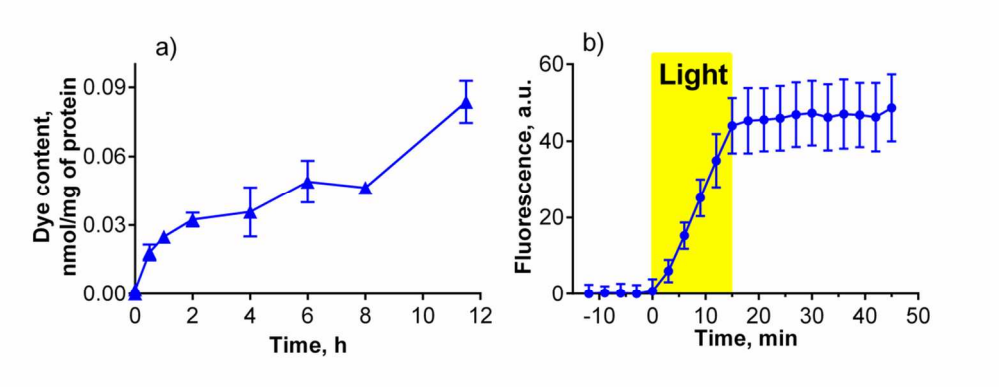

a) Cellular uptake of compound 6 by HeLa cells after incubation with 4 μM 6. The experiments were performed in duplicate. b) Increase in the fluorescence of 5(6)-chloromethyl-2′,7′-dichlorofluorescein (λex = 485 nm, λem = 525 nm) after the photodynamic treatment of HeLa cells incubated with 6. The results were corrected for autoxidation by subtracting the light and dark controls. The experiments were performed in triplicate.

Fig. 5

54x21mm (600 x 600 DPI)

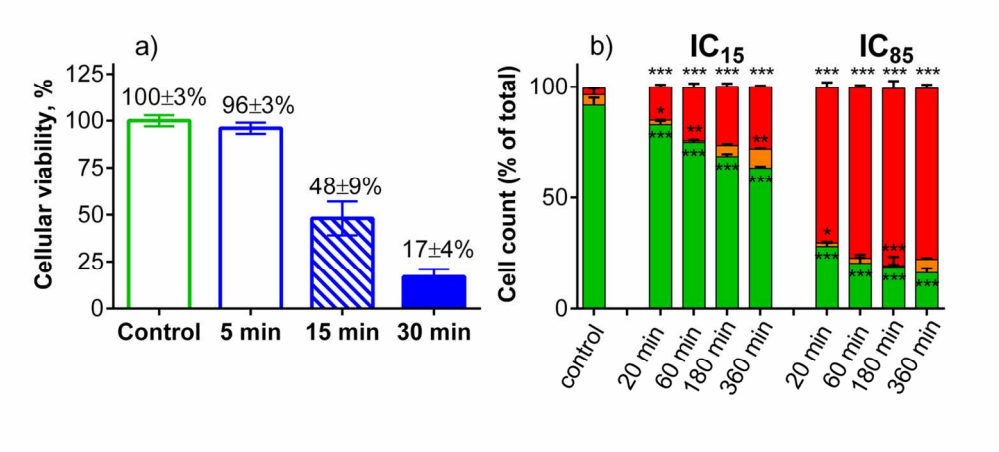

a) Viability of HeLa cells as a function of the light dose following photodynamic treatment with 6 (3.8 nM); green open bar, control cells (without 6 in the presence of light); blue open bar, 5 min of irradiation (total fluence 3.7 J cm−2); blue dashed bar, 15 min of irradiation (11.2 J cm−2); blue full bar, 30 min of irradiation (22.3 J cm−2). The experiments were performed in duplicate. b) Flow cytometry assessment of the HeLa cell death mode for 6 analysed at different times after irradiation at concentrations corresponding to the EC15 and the EC85, expressed as the cell count based on the annexin V−Alexa Fluor 488 or/and PI positivity. Non-apoptotic cells (green), apoptotic cells (orange), late apoptosis/early necrosis (red). The experiments were performed in triplicate. *, $p < 0.05$; **, $p < 0.01$; ***, $p < 0.001$.

Fig. 6

63x28mm (600 x 600 DPI)

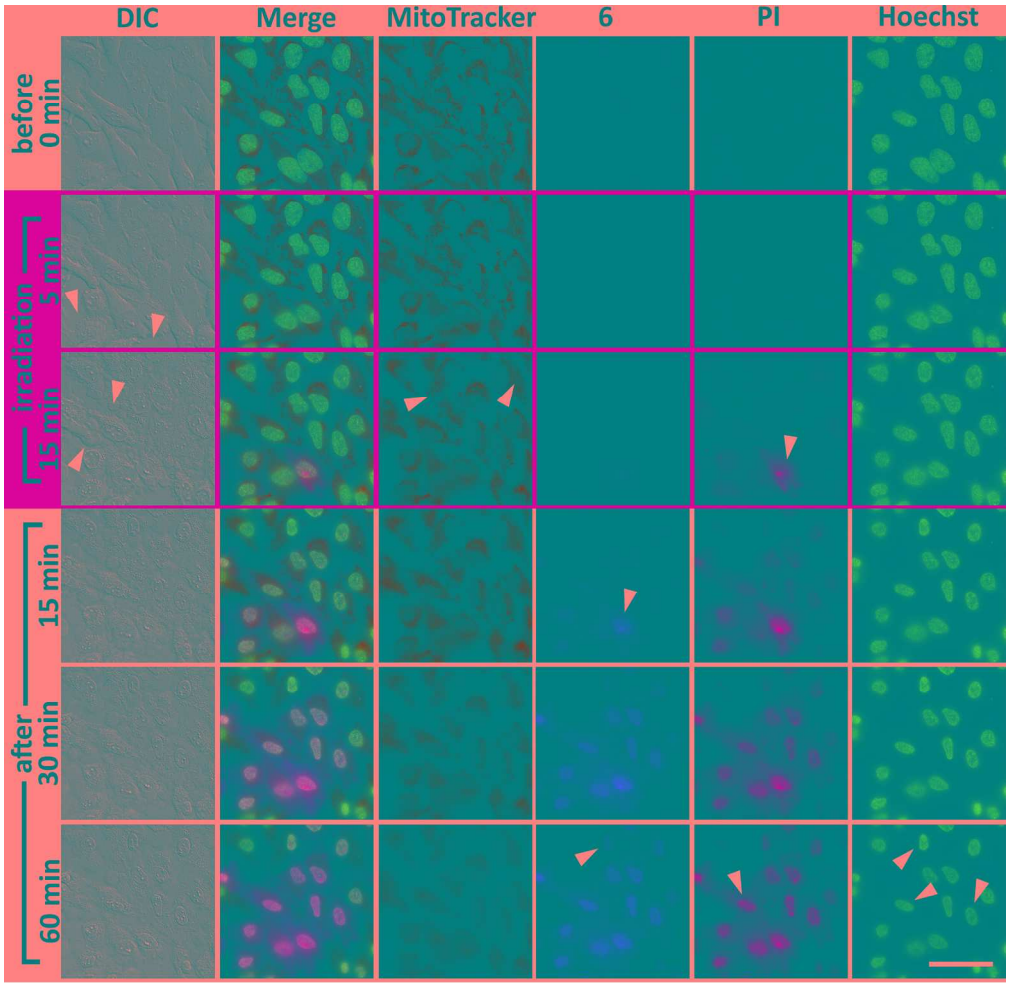

Changes in the morphology of HeLa cells treated with 6 during and after irradiation. The nuclei were visualized with Hoechst 33342 (Hoechst) and propidium iodide (PI); the mitochondria were visualized by MitoTracker Green. The arrows indicate important details discussed in the text. DIC = differential interference contrast. Bar represents 200 μm.

Fig. 7

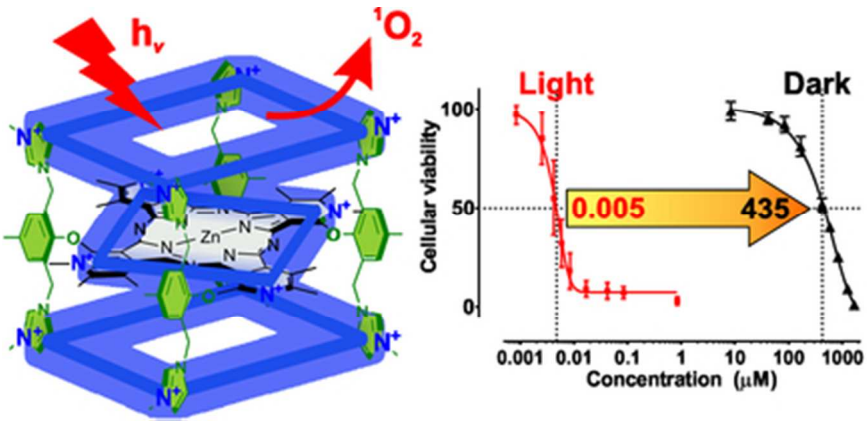

Graphical abstract

38x17mm (300 x 300 DPI)